Contents

New hybrid of Conjugate Gradient Technique for Solving Fuzzy Nonlinear Equations

[1]Hisham M. Khudhur 🆔 **, [2] Khalil K. Abbo** 🆔

[1]Mathematics Department, College of Computer Science and mathematics, University of Mosul, Mosul, Iraq,
hisham892020@uomosul.edu.iq
[2]Department of Mathematics, College of Basic Education, University of Telafer, Tall'Afar, Iraq, dr.khalil-khuder@uotelafer.edu.iq

Corresponding author: First A. Author (e-mail: hisham892020@uomosul.edu.iq).

ABSTRACT In this paper, we suggest a new technique for numerical solution of fuzzy nonlinear equations in parametric form using a new Conjugate Gradient Technique. Table of the numerical solution is given to show the efficiency of the proposed technique and which is compared with classical algorithms such as (Fletcher and Reeves (FR), Polak and Ribiere (PRP), Fletcher (CD), and (KH)) techniques.

KEYWORDS: Conjugate Gradient Technique; Fuzzy Parametric Form; Fuzzy Nonlinear Equations; Numerical Techniques; Optimization Technique; Fuzzy Interval.

1. INTRODUCTION

Simultaneous non-linear equation systems have recently played a major role in various fields of science, such as mathematics, statistics, engineering, social sciences, robot technology and medicine. The idea concept of fuzzy numbers and mathematical operation was first proposed and researched by [1-5]. The use of fuzzy numbers is important among nonlinear systems, the parameters of which are defined entirely or partially by fuzzy numbers [6-8]. Buckley and Qu are Standard analytic techniques [9][10], cannot be adapted to the solution of equations such as

i- $ax^5 + bx^4 + cx^3 + dx - e = f$,

ii- $x - \sin(x) = g$,

Where x, a, b, c, d, e, f and g are fuzzy numbers. In this way, we need to build up the numerical techniques to find the roots of such equations. Here, we think about these conditions, as a rule, as

$F(x) = c.$

whose parameters are all or partially represented by fuzzy numbers, [11] research the performance of Newton's scheme for getting the solve of the fuzzy nonlinear equations and reached out to systems of fuzzy nonlinear equations by [12]. Newton's technique converges quickly if the initial point is picked near the solution point. The primary downside of Newton's strategy is figuring the Hessian matrix in each epoch. Probably the easiest variation of Newton's technique was considered by[13] for solution the double fuzzy nonlinear equations. Another type of Newton's technique known as Levenberg-Marquardt alteration was used to fathom fuzzy nonlinear equations by[14]. Authors in [15] applied also the Broyden's technique to solve the fuzzy nonlinear equations. Every one of these techniques is Newton-like which requires the calculation and storage of either Hessian matrix or approximate Hessian matrix at every iterative of iterations. Newly, a diagonal update technique for solving fuzzy nonlinear equations was proposed by[14]. A gradient based technique by [16] was applied to get the optimal value of variables of fuzzy nonlinear equations. This technique is simple and requires no Hessian matrix assessment during calculations. Be that as it may, technique convergence is linear and very slow toward

the optimal solution [17-19]. The steepest descent technique is additionally affected by ill-conditioning [20,21].

In this work we developed a new conjugate gradient coefficient and applied it to solve fuzzy nonlinear equations. The conjugate gradient technique is known to be easy and high proficient in taking care of optimization problem. The plan in this work is to convert the parametric form of a fuzzy nonlinear equation into an unconstrained optimization problem before applying the new conjugate gradient technique to get the optimal solution.

This paper is organized as follows: In Section 2. Preliminaries in fuzzy. In Section 3 we present new conjugate gradient (CG) technique. Section 4 show that our technique satisfies descent and global convergence conditions. Section 5 presents numerical experiments and comparisons.

2. PRELIMINARIES

Definition 1. A fuzzy number is a fuzzy set like $u: \mathbb{R} \longrightarrow I = [0,1]$ which satisfies[22, 23],
1. u is upper semi continuous,
2. $u(x) = 0$ outside some interval $[c, d]$,
3. There are real numbers a, b such that $c \leq a \leq b \leq d$ and
  i. $u(x)$ is monotonic increasing on $[c, a]$,
  ii. $u(x)$ is monotonic decreasing on $[b, d]$,
  iii. $u(x) = 1, a \leq x \leq b$.
The set of all these fuzzy numbers is denoted by E. An equivalent parametric is also given in[24] as follows.

Definition 2. A fuzzy number u in parametric form is a pair $(\underline{u}, \overline{u})$ of function $\underline{u}(r), \overline{u}(r), 0 \leq r \leq 1$, which satisfies the following requirements:

1- $\underline{u}(r)$ is a bounded monotonic increasing left continuous function,
2- $\overline{u}(r)$ is a bounded monotonic decreasing left continuous function,
3- $\underline{u}(r) \leq \overline{u}(r), 0 \leq r \leq 1$.
 A popular fuzzy number is the trapezoidal fuzzy number $u = (x_0, y_0, \sigma, \beta)$ with interval defuzzifier $[x_0, y_0]$ and left fuzziness σ and right fuzziness β where the membership function is

$$u(x) = \begin{cases} \dfrac{1}{\sigma}(x - x_0 + \sigma), & x_0 - \sigma \leq x \leq x_0, \\ 1, & x \in [x_0, y_0], \\ \dfrac{1}{\beta}(y_0 - x + \beta), & y_0 \leq x \leq y_0 + \beta, \\ 0, & otherwise. \end{cases}$$

Its parametric form is

$$\underline{u}(r) = x_0 - \sigma + r\sigma, \overline{u}(r) = y_0 + \beta + r\beta.$$

Let $TF(\mathbb{R})$ be the set of all trapezoidal fuzzy numbers. The addition and scalar multiplication of fuzzy numbers are defined by the extension principle and can be equivalently represented as follows.

For arbitrary $u = (\underline{u}, \overline{u}), v = (\underline{v}, \overline{v})$ and $k > 0$ we define addition $(u + v)$ and multiplication by scalar k as

$$\left(\underline{u} + \underline{v}\right)(r) = \underline{u} + \underline{v}, \quad (\overline{u} + \overline{v}) = \overline{u} + \overline{v}, \tag{1}$$

$$\left(\underline{ku}\right)(r) = ku(r), \quad \left(\overline{ku}\right)(r) = k\overline{u}(r). \tag{2}$$

3. NEW CONJUGATE GRADIENT TECHNIQUE FOR SOLVING FUZZY NONLINEAR EQUATIONS

In this section we will show some of the conjugate gradient techniques and then suggest a new algorithm for conjugate gradient algorithm for solving fuzzy nonlinear equations

$$x_{k+1} = x_k + \alpha_k d_k, \quad k \geq 1 \tag{3}$$

Where α_k step-size that satisfy the standard wolfe conditions

$$f(x_k + \alpha_k d_k) \leq f(x_k) + \delta\alpha_k g_k^T d_k \tag{4}$$

$$d_k^T g(x_k + \alpha_k d_k) \geq \sigma d_k^T g_k \tag{5}$$

or strong Wolfe conditions

$$f(x_k + \alpha_k d_k) \leq f(x) + \delta\alpha_k g_k^T d_k \tag{6}$$

$$|d_k^T g(x_k + \alpha_k d_k)| \leq -\sigma d_k^T g_k \tag{7}$$

$$d_{k+1} = \begin{cases} -g_1, & k = 1 \\ -g_{k+1} + \beta_k d_k, & k \geq 1 \end{cases} \tag{8}$$

The Fletcher and Reeves (FR) [25], Fletcher (CD) [26], Polak and Ribiere (PRP) [27] and β is scalar.

$$\beta^{FR} = \frac{\|g_{k+1}\|^2}{\|g_k\|^2}, \text{ see [25]}$$

$$\beta^{CD} = \frac{-\|g_{k+1}\|^2}{g_k^T d_k}, \text{ see [26]}$$

$$\beta^{PRP} = \frac{g_{k+1}^T y_k}{\|g_k\|^2}, \text{ see [27]}$$

Where $g_k = \nabla f(x_k)$, and let $y_k = g_{k+1} - g_k$.

Now we suggest a new of conjugate gradient algorithm for solving fuzzy nonlinear equations depend basically on norm-1 instead of norm-2 in Fletcher-Reeves (FR) algorithm so we get new formula

$$d_{k+1} = -g_{k+1} + \beta_k^{NEW} d_k \tag{9}$$

$$\beta_k^{KH} = \frac{\|g_{k+1}\|_1^2}{\|g_k\|_1^2} \text{ see [28]}$$

$$\beta_k^{NEW} = \theta_k \beta_k^{FR} + (1 - \theta_k)\beta_k^{KH} \tag{10}$$

Multiply the equation (9) by y_k
$$y_k^T d_{k+1} = -y_k^T g_{k+1} + \beta_k^{NEW} y_k^T d_k$$
By Pure Conjugacy Condition we get

$$-y_k^T g_{k+1} + \beta_k^{NEW} y_k^T d_k = 0$$

$$-y_k^T g_{k+1} + (\theta_k \beta_k^{FR} + (1 - \theta_k)\beta_k^{KH}) y_k^T d_k = 0$$

3

$$(\theta_k(\beta_k^{FR} - \beta_k^{KH}) + \beta_k^{KH})y_k^T d_k = y_k^T g_{k+1}$$

$$\theta_k(\beta_k^{FR} - \beta_k^{KH}) = \frac{y_k^T g_{k+1}}{y_k^T d_k} - \beta_k^{KH}$$

$$\theta_k = \frac{(y_k^T g_{k+1} \parallel g_k \parallel_1^2 - y_k^T d_k \parallel g_{k+1} \parallel_1^2) \parallel g_k \parallel^2}{(\parallel g_{k+1} \parallel^2 \parallel g_k \parallel_1^2 - \parallel g_{k+1} \parallel_1^2 \parallel g_k \parallel^2)y_k^T d_k} \qquad (11)$$

substituting (11) in (10).

Algorithm (NEW)

Step (1): Initialization:

choose $x_1 \in R^n$ and calculate $f(x_1), g(x_1)$ and consider

$d_1 = -g_1$ and $k = 1$

Step (2): Check for convergent:

If $\parallel g_k \parallel \leq \varepsilon$, stop, x_k is the optimum solution

else go to step(3).

Step (3): line search:

Calculate α_k satisfying the strong Wolfe conditions and update variable $x_{k+1} = x_k + \alpha_k d_k$. Compute, $f_{k+1}, g_{k+1}, g_k, d_k$.

Step (4): Calculate direction search:

Calculate β_k from (10) and then calculate

$d_{k+1} = -g_{k+1} + \beta_k^{NEW} d_k$ then $k = k + 1$ go to step (2).

4. THE DESCENT PROPERTY AND GLOBAL CONVERGENCE STUDY OF NEW TECHNIQUE

This technique is developed satisfy The Descent Property and Global convergence because the β_k^{FR} & $\frac{\parallel g_{k+1} \parallel_1^2}{\parallel g_k \parallel_1^2}$ satisfies the conditions Descent Property and Global convergence Because β_k^{NEW} it is derived from them see more [25-33].

5. NUMERICAL EXAMPLES

In this part, we present the numerical solution of some examples using the new proposed technique for CG technique for fuzzy nonlinear equations. All computations are carried out on MATLAB 9.0 using a double precision computer. We use the stop criterion $\parallel g_{k+1} \parallel < 10^{-6}$, We

employ the new technique to solve fuzzy nonlinear equations .and compare with the other techniques (Fletcher and Reeves (FR), Polak and Ribiere (PRP), Fletcher (CD) and (KH)).

Example 1: Consider the fuzzy nonlinear equation [9]

$(3,4,5)x^2 + (1,2,3)x = (1,2,3)$

Without any loss of generality, assume that x is positive, and then the parametric form of this equation is as follows:

$$\begin{cases} (3+r)\underline{x}^2(r) + (1+r)\underline{x}(r) - (1+r) = 0, \\ (5-r)\overline{x}^2(r) + (3-r)\overline{x}(r) - (3-r) = 0. \end{cases}$$

The above system needs initial values as follows. For $r = 1$

$$\begin{cases} 4\underline{x}^2(1) + 2\underline{x}(1) - 2 = 0, \\ 4\overline{x}^2(1) + 2\overline{x}(1) - 2 = 0, \end{cases}$$

For $r = 0$

$$\begin{cases} 3\underline{x}^2(0) + \underline{x}(0) - 1 = 0, \\ 5\overline{x}^2(0) + \overline{x}(0) - 3 = 0 \end{cases}$$

With initial values

$x_0 = (\underline{x}(0), \underline{x}(1), \overline{x}(1), \overline{x}(0)) = (0.434, 0.5, 0.5, 0.681)$.

Example 2: Consider the fuzzy nonlinear equation [9]

$(4,6,8)x^2 + (2,3,4)\,x - (8,12,16) = (5,6,7)$

Without any loss of generality, assume that x is positive, and then the parametric form of this equation is as follows:

$$\begin{cases} (4+2r)\underline{x}^2(r) + (2+r)\underline{x}(r) - (3+3r) = 0, \\ (8-2r)\overline{x}^2(r) + (4-r)\overline{x}(r) - (9-3r) = 0. \end{cases}$$

The above system needs initial values as follows. For $r = 1$

$$\begin{cases} 6\underline{x}^2(1) + 3\underline{x}(1) - 6 = 0, \\ 6\overline{x}^2(1) + 3\overline{x}(1) - 6 = 0, \end{cases}$$

For $r = 0$

$$\begin{cases} 4\underline{x}^2(0) + 2\underline{x}(0) - 3 = 0, \\ 8\overline{x}^2(0) + 4\overline{x}(0) - 9 = 0, \end{cases}$$

With initial values

$x_0 = (\underline{x}(0), \underline{x}(1), \overline{x}(1), \overline{x}(0)) = (0.651, 0.7808, 0.7808, 0.8397)$.

Example 3: Consider the fuzzy nonlinear equation [9]

$(1,2,3)x^3 + (2,3,4)x^2 + (3,4,5) = (5,8,13)$

Without any loss of generality, assume that x is positive, and then the parametric form of this equation is as follows:

$$\begin{cases} (1+r)\underline{x}^3(r) + (2+r)\underline{x}^2(r) - (2+2r) = 0, \\ (3-r)\overline{x}^3(r) + (4-r)\overline{x}^2(r) - (8-4r) = 0. \end{cases}$$

The above system needs initial values as follows. For $r = 1$

$$\begin{cases} 2\underline{x}^3(1) + 3\underline{x}^2(1) - 4 = 0, \\ 2\overline{x}^3(1) + 3\overline{x}^2(1) - 4 = 0, \end{cases}$$

For $r = 0$

$$\begin{cases} \underline{x}^3(0) + 2\underline{x}^2(0) - 2 = 0, \\ 3\overline{x}^3(0) + 4\overline{x}^2(0) - 8 = 0. \end{cases}$$

With initial values

$x_0 = (\underline{x}(0), \underline{x}(1), \overline{x}(1), \overline{x}(0)) = (0.76, 0.91, 0.91, 1.06)$.

Table of numerical results for examples above

Example	FR			PRP			CD			β_k^{KH}			NEW2		
	iter	x_optimal	f_optimal	iter	x_optimal	f_optimal	iter	x_optimal	f_optimal	iter	x_optimal	f_optimal	iter	x_optimal	f_optimal
1	8	0.4343 0.5000 0.5000 0.5307	5.2505e-014	6	0.4343 0.5000 0.5000 0.5307	1.2314e-016	8	0.4343 0.5000 0.5000 0.5307	8.1709e-014	6	0.4343 0.5000 0.5000 0.5307	1.7016e-011	5	**0.4343 0.5000 0.5000 0.5307**	**8.6657e-016**
2	12	0.6514 0.7808 0.7808 0.8397	2.3998e-010	12	0.6514 0.7808 0.7808 0.8397	7.9887e-012	14	0.6514 0.7808 0.7808 0.8397	5.9506e-010	9	**0.6514 0.7808 0.7808 0.8397**	**1.9513e-011**	9	**0.6514 0.7808 0.7808 0.8397**	**7.7858e-011**
3	19	0.8393 0.9108 0.9108 1.0564	2.6011e-011	16	0.8393 0.9108 0.9108 1.0564	4.6595e-012	135	0.8393 0.9108 0.9108 1.0564	1.4978e-008	13	0.8393 0.9108 0.9108 1.0564	1.6756e-013	9	**0.8393 0.9108 0.9108 1.0564**	**1.2232e-012**

Iter   :   *Numbers Iterations.*

x_optimal   :   *Optimal of x value.*

f_optimal   :   *Optimal of f value.*

6. CONCLUSIONS

We presented in this research a new hybrid conjugate gradient technique for solving fuzzy nonlinear equations, and the proposed algorithm has shown a high efficiency in solving these problems with the least number of iterations and higher accuracy in reaching the approximate solution of the function.

Acknowledgements

REFERENCES

[1]   S. S. L. Cheng and L. A. Zadeh, "On fuzzy mapping and control," *IEEE Trans. Syst. Man Cybern.*, vol. 2, pp. 30–34, 1972.

[2]   D. Dubois and H. Prade, "Operations on fuzzy numbers," *Int. J. Syst. Sci.*, vol. 9, no. 6, pp. 613–626, 1978.

[3]   M. Mizumoto, "Some properties of fuzzy numbers," 1979.

[4]   S. Nahmias, "Fuzzy variables," *Fuzzy sets Syst.*, vol. 1, no. 2, pp. 97–110, 1978.

[5]   L. A. Zadeh, "The concept of a linguistic variable and its application to approximate reasoning—II," *Inf. Sci. (Ny).*, vol. 8, no. 4, pp. 301–357, 1975.

[6]   Y. J. Cho, N. J. Huang, and S. M. Kang, "Nonlinear equations for fuzzy mappings in probabilistic normed spaces," *Fuzzy Sets Syst.*, vol. 110, no. 1, pp. 115–122, 2000.

[7]   J. Fang, "On nonlinear equations for fuzzy mappings in probabilistic normed spaces," *Fuzzy Sets Syst.*, vol. 131, no. 3, pp. 357–364, 2002.

[8]   J. Ma and G. Feng, "An approach to H∞ control of fuzzy dynamic systems," *Fuzzy Sets Syst.*, vol. 137, no. 3, pp. 367–386, 2003.

[9]   J. J. Buckley and Y. Qu, "Solving linear and quadratic fuzzy equations," *Fuzzy sets Syst.*, vol. 38, no. 1, pp. 43–59, 1990.

[10]   J. J. Buckley and Y. Qu, "Solving fuzzy equations: a new solution concept," *Fuzzy sets Syst.*, vol. 39, no. 3, pp. 291–301, 1991.

[11]   S. Abbasbandy and B. Asady, "Newton's method for solving fuzzy nonlinear equations," *Appl. Math. Comput.*, vol. 159, no. 2, pp. 349–356, Dec. 2004, doi: 10.1016/j.amc.2003.10.048.

[12]   A. Mottaghi, R. Ezzati, and E. Khorram, "A new method for solving fuzzy linear programming problems based on the fuzzy linear complementary problem (FLCP)," *Int. J. Fuzzy Syst.*, vol. 17, no. 2, pp. 236–245, 2015.

[13]   M. Y. Waziri and A. U. Moyi, "An alternative approach for solving dual fuzzy nonlinear equations," *Int. J. Fuzzy Syst.*, vol. 18, no. 1, pp. 103–107, 2016.

[14]   I. Mohammed Sulaiman, M. Mamat, M. Yusuf Waziri, and N. Shamsidah Amzeh, "Barzilai-Borwein gradient method for solving fuzzy nonlinear equations," *Int. J. Eng. Technol.*, vol. 7, no. 3.28, p. 80, 2018, doi: 10.14419/ijet.v7i3.28.20972.

[15]   M. Mamat, A. Ramli, and M. L. Abdullah, "Broyden's method for solving fuzzy nonlinear equations," *Adv. Fuzzy Syst.*, 2010, doi: 10.1155/2010/763270.

[16]   S. Abbasbandy and A. Jafarian, "Steepest descent method for solving fuzzy nonlinear equations," *Appl.*

Math. Comput., vol. 174, no. 1, pp. 669–675, Mar. 2006, doi: 10.1016/j.amc.2005.04.092.

[17] E. K. P. Chong and S. H. Zak, *An introduction to optimization*. John Wiley & Sons, 2004.

[18] K. K. Abbo, Y. A. Laylani, and H. M. Khudhur, "Proposed new Scaled conjugate gradient algorithm for Unconstrained Optimization," *Int. J. Enhanc. Res. Sci. Technol. Eng.*, vol. 5, no. 7, 2016.

[19] K. K. ABBO, Y. A. Laylani, and H. M. Khudhur, "A NEW SPECTRAL CONJUGATE GRADIENT ALGORITHM FOR UNCONSTRAINED OPTIMIZATION," *Int. J. Math. Comput. Appl. Res.*, vol. 8, pp. 1–9, 2018, [Online]. Available: www.tjprc.org.

[20] W. Sun and Y.-X. Yuan, *Optimization theory and methods: nonlinear programming*, vol. 1. Springer Science & Business Media, 2006.

[21] H. N. Jabbar, K. K. Abbo, and H. M. Khudhur, "Four--Term Conjugate Gradient (CG) Method Based on Pure Conjugacy Condition for Unconstrained Optimization," *kirkuk Univ. J. Sci. Stud.*, vol. 13, no. 2, pp. 101–113, 2018.

[22] D. J. Dubois, *Fuzzy sets and systems: theory and applications*, vol. 144. Academic press, 1980.

[23] L. A. Zadeh, "Fuzzy sets," *Inf. Control*, vol. 8, no. 3, pp. 338–353, 1965.

[24] R. Goetschel Jr and W. Voxman, "Elementary fuzzy calculus," *Fuzzy sets Syst.*, vol. 18, no. 1, pp. 31–43, 1986.

[25] R. Fletcher and C. M. Reeves, "Function minimization by conjugate gradients," *Comput. J.*, vol. 7, no. 2, pp. 149–154, 1964, doi: 10.1093/comjnl/7.2.149.

[26] L. C. W. Dixon, "Conjugate gradient algorithms: quadratic termination without linear searches," *IMA J. Appl. Math.*, vol. 15, no. 1, pp. 9–18, 1975.

[27] E. Polak and G. Ribiere, "Note sur la convergence de méthodes de directions conjuguées," *ESAIM Math. Model. Numer. Anal. Mathématique Anal. Numérique*, vol. 3, no. R1, pp. 35–43, 1969.

[28] Hisham M. Khudhur; Khalil K. Abbo, "A New Type of Conjugate Gradient Technique for Solving Fuzzy Nonlinear Algebraic Equations", in Ibn Al-Haitham 2nd International Conferencefor Pure and Applied Sciences (IHICPAS)- 2020 (Baghdad-Iraq 9-10 December 2020: iop, 2020).

[29] H. M. Khudhur, "Numerical and analytical study of some descent algorithms to solve unconstrained Optimization problems," University of Mosul, 2015.

[30] K. K. Abbo and H. M. Khudhur, "New A hybrid conjugate gradient Fletcher-Reeves and Polak-Ribiere algorithm for unconstrained optimization," *Tikrit J. Pure Sci.*, vol. 21, no. 1, pp. 124–129, 2015.

[31] K. K. Abbo and H. M. Khudhur, "New A hybrid Hestenes-Stiefel and Dai-Yuan conjugate gradient algorithms for unconstrained optimization," *Tikrit J. Pure Sci.*, vol. 21, no. 1, pp. 118–123, 2015.

[32] Y. A. Laylani, K. K. Abbo, and H. M. Khudhur, "Training feed forward neural network with modified Fletcher-Reeves method," *J. Multidiscip. Model. Optim.*, vol. 1, no. 1, pp. 14–22, 2018, [Online]. Available: http://dergipark.gov.tr/jmmo/issue/38716/392124#article_cite.

[33] Z. M. Abdullah, M. Hameed, M. K. Hisham, and M. A. Khaleel, "Modified new conjugate gradient method for Unconstrained Optimization," *Tikrit J. Pure Sci.*, vol. 24, no. 5, pp. 86–90, 2019.

Kinematic Analysis of Open-Source 5 Degree of Freedom Robot Arm

Mehmet Gül

Computer Engineering Department, Şırnak University, Turkey

Corresponding author: First A. Author (e-mail: mgul@sirnak.edu.tr; mehmetgul@ymail.com).

ABSTRACT Today, it is especially estimated that robots will be more than 2 million between 2018-2021, with their increasing use in the industry, in the world. In the industrial environment, robots are used to neutralize toxic substances, explosives, or to replace certain repetitive tasks in the industry for human intervention. On the other hand, robotic systems are used in different areas such as office environment, military duties, and use in hospital environments. It is widespread the use of open-source design robot day by day, in addition to the increasing use of robots, which have invaluable effective uses in complex or dangerous processes. The use of open-source robotic systems is cheaper, developable, and has no usage restrictions due to copyright compared to equivalent robots used in the industry. For these reasons, in our study, a robotic arm with 5 degrees of freedom, printed with 3D printers at industrial scales, was developed. The printed robotic arm was developed to be used as an auxiliary equipment for hospital staff, especially in today's hospital environment. Kinematic analysis is required to determine the working space of the developed robotic arm. The working space of the robotic arm, which is intended to be used as auxiliary equipment in the hospital environment, was revealed by kinematic analysis.

KEYWORDS: Robotic Arm, Forward Kinematic, Inverse Kinematic

1. INTRODUCTION

The effects of developing technological innovations on our daily lives are increasing significantly. The example of these innovations is the prevalence of robots in our daily lives. The applications of robots can be listed in many areas such as office environment, military duties, hospital operations, hazardous environment, and agricultural practices. For instance, robots are indispensable in difficult or dangerous processes such as instead of human intervention to explosive chemicals, neutralizing bombs, or some special repetitive tasks in industries. Therefore, a robot can replace man to do work [1]. Robots perform very critical tasks in the machining and assembly of turbine blades, impellers, and parts with large composite surfaces. These processes are very hard for any workers especially in the aviation and automotive industry. Today, the usage of robots is at most 5% all over the world in the industry [2]. According to The International Federation of Robotics (IFR) data, this usage rate is estimated to be more than 2 million in the world between 2018 and 2021 [3].

Robots can be operated in many ways and can perform the desired tasks completely. It is the most important reason for the preferences. The programmed robots are inevitable to perform the given task whether simple or complex tasks. Robots are controllable and traceable only if in the working space. Different methods are used to monitor robot location within the working space. In conventional systems, feedback is usually made by calculating the angular values obtained from rotary encoders fixed to the

joints. In advanced systems, an optical measuring device is used to calculate direct feedback for cooperative robots. Unlike conventional robot systems, the position of the robot is determined by the IR sensor and color sensor. The robotic arm can be directed to select and displace any object which position is known in the working space [4, 5].

On the other hand, the position control of the robot arm is significant for tracking the given mission. For instance, an arrangement of robot arms can assume a role in selecting and sorting various objects placed in a common working space. Notwithstanding knowing the situation of items in this working space, it is necessary to perform motion planning of the maneuvers to grasp the objects [6, 7]. These stages are required for robotic systems and it is conceivable with control policy and kinematic calculations.

Kinematics and control policy are important in robotic systems for collaborative workings. It is extremely important to know the positions and power of the robot arms to establish and design an effective system [8, 9]. It is currently witnessed the widespread usage of the robotic system in many aspects because of the indispensable features of the robotic system. In the last quarter-century, the robotic system is used in the field of health, in particular, as assistant robots, therapy robots, or surgical robots. Laparoscopic robots such as daVinci are examples of the robotic systems used in surgical operations [10 – 12].

In laparoscopic operations, precision is extremely significant. In robot-assisted surgical operations, while the primary surgeon remotely controls the robotic arms beside the patients' bed through the surgical console, the assistant surgeon assists the first surgeon to utilize the accessory port of the daVinci system [10, 13]. The use of the robotic surgical system can diminish the expenses of surgical operations as well as the most effective use of manpower [14].

In the hospital, there isn't always such a complicated task, in some cases, only the auxiliary robotic system can be required. For such cases, the robot arm may be manually controlled rather than autonomously controlled. It is important to decrease the workforce of hospital employees particularly in expanding infections such as corona-virus pandemics. For instance, more than one employee is required to perform the appropriate assessment of an obese patient in tasks such as adjusting the location of the MRI imaging or CT imaging. In such cases, the requisite maneuver can be provided to the obese patient with the assistance of a manually controllable robot arm. In this study, the robot arm with 5 degrees of freedom (DoF) was obtained from the 3D printer. Its kinematic analysis was done to determine working space of robot arm.

2. SYSTEM ARCHITECTURE

2.1 POWER SUPPLY

The used power supply provided the power needed for the movement of the robot arm. It provided 24V voltage and 12.5A current required for the movement, whether it supplied the required power from the

battery or AC source. Strong power supply satisfied the power of the used stepper motor which was different properties for the movement of the robot arm such as Nema 23 stepper motor.

2.2 MOTHERBOARD

The robot arm was controlled with MKS Gen V1.4. MKS uses the 8-bit AVR RISC-based ATmega2560 microchip, which also stands out with its low power consumption with its advanced RISC architecture. There is a self-programmable flash memory for the 256KB system on the ATmega2560 microprocessor. Flash memory offers very high performance for the microcontroller. The microprocessor also has 8KB Ram and 4 KB SRAM. The microprocessor 4KB EEPROM, which stands out with its 16MHz operating speed, allows storing long character strings and hundreds of settings data of an advanced system. There are 100 pins on the microprocessor, 86 of the pins allow I/O to input and output data. It also includes 4 USART and Master / Slave SPI serial interfaces for the 16 channel 10 bit-ADC converter.

In addition to the high-performance microprocessor, it contains integrated Ramps a developer-friendly advantage card, and Ramps compatible firmware. On the other hand, it can be controlled via an LCD board with a display port. It also contains smart-controller features with an SD card connector. There are three AUX ports on the motherboard and three Servo motor control ports too. There are 5V and 12V output voltage on the motherboard and also this motherboard withstand voltage between 12V and 24V. It has a short circuit with the recoverable fuse. Five motors are controlled on this motherboard with its extended connection points [16, 17].

2.3 MOTOR DRIVER

The TB6560 motor driver was used for the movement of the manipulators. It provides high performance especially in the movement of high current and voltage stepper motors. It can withstand 35V regression and 3A current. It has 4 phase stepper motor driving capacity. The aluminum heatsink on the drive allows the heat on the chip to be dissipated quickly. Thanks to the cooler, the system shutdown is prevented [18].

The TB6560 motor driver is used in the robot arm system and it uses the Toshiba TB6560AHQ chip. It is a preferred driver especially for the operation of two-phase bipolar stepper motors. Even high-profile stepper motors such as Nema 23 are controlled with the 3A provided by the drive. The chip on the drive has many security functions such as overcurrent, low voltage shutdown, and overheat protection. On the other hand, despite all the precautions, there is no voltage protection on the drive. The optimum voltage value for the driver is 24V voltage, however, it can even stand 10V-35V voltage range. The drive also has a capacity that can withstand up to 3.5A current, while the optimum operating current is 3A current. The sensitivity range of the driver, which has options such as motor step control, is in the range of 1, 1/2, 1/8, 1/16 micro-step. The driver also maintains current control to prevent the motors that it controls from overcurrent. The current control rate is 100%, 75%, 50% and 25% [19, 20].
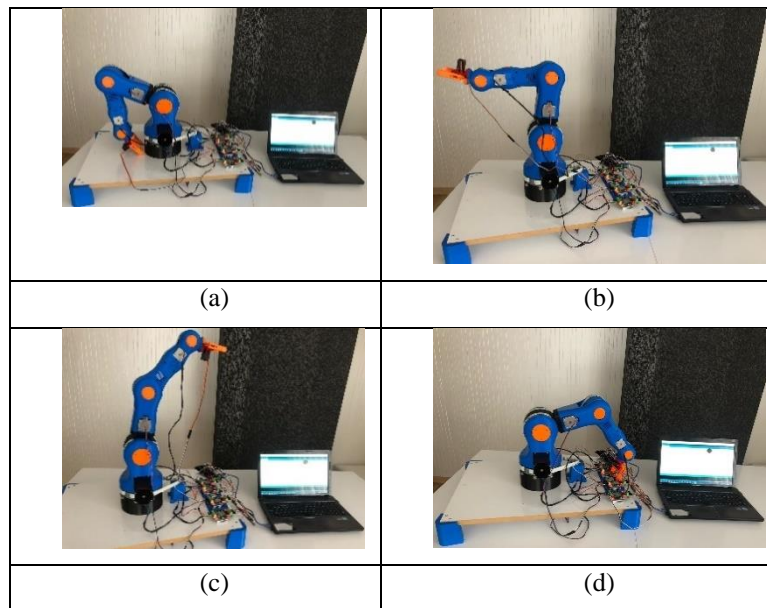
2.4 STEPPER MOTOR

Stepper motors take a very important role among known motors. It is widely used especially in measurement and control applications, robot applications, CNC applications, etc. [21].

3. APPLICATION

3.1 ROBOT ARM

The open-source BCN3D Moveo robot arm was used from its webpage and it was obtained by printing from a 3D printer. The robot arm has one horizontal and 3 vertical moving axes. Stepper motors and motor drivers actualize two dimensions horizontal and vertical displacement of the robot arm manipulators. The developed robot arm can access any objects in the working space because the horizontal angle of rotational is more than 180 degrees and the first vertical axis has a rotation angle of 220 degrees. The only thing to do for this is to program the horizontal axis with a rotation angle of at least 180 degrees. Simulation is shown in the figure below (figure 1).

For instance, it can be used ancillary robot systems in a hospital environment in a situation like pandemic corona-virus today. It is important to be open source and to be developed as a model.

(a)	(b)
(c)	(d)

Figure 1: Open-source robot arm

If the strength of the robot arm components is increased, it will be gotten more strength robotic systems printed with 3D printers, especially according to the variety of the material used during printing. For example, the strength of the carbon fiber filament is harder than the PLA filament, which is common to use. In this case, robotic systems with high joint strength can be used. The use of open source designed robotic systems is getting widespread every day [22]. The widespread robotic systems are prepared through design programs such as SolidWorks, and then the assembly simulation can be previewed for the robotic system.

The movement of the robot arm is controlled by a motherboard using an Arduino compatible ATmega2560 processor. The feature of the used motherboard does the joint movements step-by-step. The disadvantage of the study is the fact that more than one joint movement cannot be done simultaneously. In the next stage of this study, it will be performed with the motherboard which enables multi-joint movement simultaneously.

3.2 ROBOT ARM KINEMATIC ANALYZE

Kinematic analysis of the robot arm is to analyze the motion geometry according to the time function by referring to the coordinate system. Forward kinematic analysis is the definition of the joint points and vector of a particular manipulator. It is additionally called the analysis process required for the position and direction of the endpoint relative to the fixed axis sets through the defined parameters of all manipulators within the robot arm. On the other hand, inverse kinematic analysis is the analysis of the accessibility and even the accessibility of the determined endpoint to the desired position with the arm parameters on the fixed reference axis set.

The difficulty of inverse kinematics analysis from robotic systems is due to the complexity of nonlinear problems utilized in the analysis. Compared to inverse kinematics analysis, there is no such difficulty in forward kinematics analysis. Nonlinear equations cannot also be combined and don't have any unique solutions. In other words, mathematical equations can emerge that can't be solved physically [23]. In the study, it was analyzed that the kinematic analysis of an industrial scale professional robot arm delivered from an open-source with 5 Degree of Freedom (DoF) degree of freedom and printed 3D printer. The robot arm is placed on a fixed base and therefore the coordinate frame assignment is shown in figure 2.
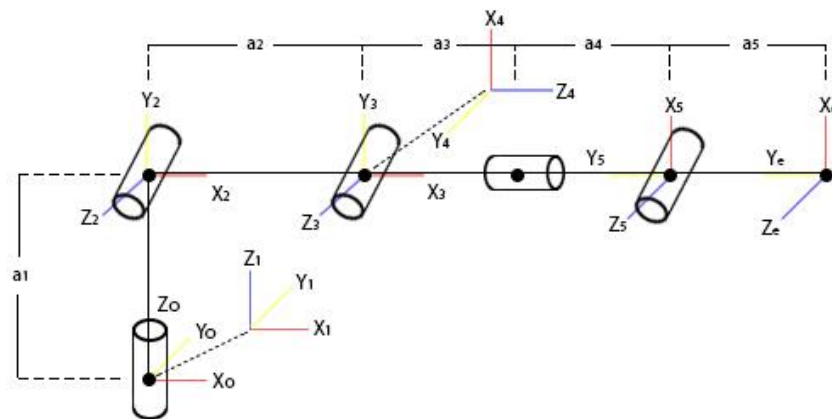

Figure 2: Coordinate frame of robot arm

3.3 FORWARD KINEMATIC ANALYZE AND HOMOGENOUS TRANSFORMATIONS

Kinematic analysis is to perform to determine the end effector location depending on the degree of freedom of the robot arm. Likewise, the working space is significantly determined by the position of

end effector on the coordinate axis within forward kinematic analysis. The analytical method or D-H method is the most common method used for forward kinematic analysis [24]. Figure 2 shows the rotational joints of each robot axis with 5 DoF, and a transformation matrix is to define the relationship between the adjacent joint on the coordinate system of each joint. It is shown as $^{i-1}_iT$ by the transformation matrix of the relationship between the two neighbors. Here i indicates the joint number. The transformation matrix between the mainframe and the endpoint of the robot arm is shown below.

Table 1: Homogenous transformation

	θ	α	a	d
1	θ_1	90	0	a_1
2	θ_2	0	a_2	0
3	0	90	0	0
4	θ_4	90	$a_3 + a_4$	0
5	θ_5	0	a_5	0

The location of the joints and the directions of rigid bodies can be defined by coordinate systems fixed according to the joints [25]. For this reason, it was deemed necessary to ascertain a coordinate system on each active joint. It is shown in figure 2 the coordinate system of the BCN3D Moveo open-source robot arm [26]. The coordinate system of the robotic arm is created with the coordinate system 1 and coincides with the basic coordinate system 0. For convenience, the Z-axis is parallel to the axis of every rotational joint, and the direction of the Z-axis is defined by the direction of rotation traditionally fixed by the right-hand rule. Each ongoing axis after the first axis is exactly consistent with the previous axis. The last axis of the system is again determined by the right-hand rule and therefore the dimension parameters in the coordinate system are shown in the figure 2.

According to the homogeneous transformation formula

$$^{i-1}_iT = \begin{bmatrix} & ^{i-1}_iR & & D \\ 0 & 0 & 0 & 1 \end{bmatrix}$$

Then all the matrices are obtained: $^0_eT = \ ^0_1T^1_2T^2_3T^3_4T^4_5T^5_eT$. The character "e" represents the end effector on the coordinate axis, $^{i-1}_iT$ expressing the transformation relationship between coordinates i to i-1, and $^{i-1}_iR$ expressing the motion relationship between coordinate i to i-1. While calculating other matrices, the base coordinate is obtained from the transformation matrix and end effector coordinate [27, 28].

Homogeneous coordinate system of open-source robot arm

While calculating other matrices, the transformation matrix is obtained from the end-effector coordinate to the base coordinate.

$$^0_eT = \ ^0_1T^1_2T^2_3T^3_4T^4_5T^5_eT = \begin{bmatrix} n_x & o_x & a_x & p_x \\ n_y & o_y & a_y & p_y \\ n_z & o_z & a_z & p_z \\ 0 & 0 & 0 & 1 \end{bmatrix}$$

14

$$n_x = C_5(C_1C_4(C_3C_2 + S_2S_3) + S_1S_4) - C_1S_5(C_3S_2 - C_2S_3) \tag{1}$$

$$n_y = C_5(S_1C_4(C_3C_2 + S_2S_3) - C_1S_4) - S_1S_5(C_3S_2 - C_2S_3) \tag{2}$$

$$n_z = C_4C_5(C_3S_2 + C_2S_3) - S_5(C_3C_2 - S_2S_3) \tag{3}$$

$$o_x = C_1C_5(C_2S_3 - C_3S_2) - S_5(C_1C_4(C_2C_3 + S_2S_3) + S_1S_4) \tag{4}$$

$$o_y = S_1C_5(C_2S_3 - C_3S_2) - S_5(S_1C_4(C_2C_3 - S_2S_3) - C_1S_4) \tag{5}$$

$$o_z = C_5(C_2C_3 + S_2S_3) - C_4S_5(S_2C_3 + C_2S_3) \tag{6}$$

$$a_x = -S_1C_4 + C_1C_2C_3S_4 + C_1S_2S_3S_4 \tag{7}$$

$$a_y = C_1C_4 + S_1C_2C_3S_4 + S_1S_2S_3S_4 \tag{8}$$

$$a_z = S_2C_3S_4 + C_2S_3S_4 \tag{9}$$

$$p_x = C_1\big(C_3\big(C_2\big(a_{(3+4)}C_4\big) - a_5S_2S_5\big) + S_2S_3\big(a_{(3+4)}S_4 + a_5C_4S_5\big) + a_2C_2 + a_5C_2S_3S_5\big) + S_1\big(a_{(3+4)}S_4 + a_5S_4C_5\big) \tag{10}$$

$$p_y = S_1\big(C_3\big(C_2\big(a_{(3+4)}C_4\big) - a_5S_2S_5\big) + S_2S_3\big(a_{(3+4)}S_4 + a_5C_4S_5\big) + a_2C_2 + a_5C_2S_3S_5\big) - C_1\big(a_{(3+4)}S_4 + a_5S_4C_5\big) \tag{11}$$

$$p_z = a_1 + a_2S_2 + C_3\big(S_2\big(a_{(3+4)}C_4 + a_5C_4C_5\big) - a_5C_2S_5\big) + S_3\big(C_2\big(a_{(3+4)}C_4 + a_5C_4C_5\big) + a_5S_2S_5\big) \tag{12}$$

3.4 INVERSE KINEMATICS

The most significant issue in robotic system is that the difficulty in performing inverse kinematic calculations, particularly the position of the robot and the calculation of all joint angles corresponding to the position pose serious issues [27].

The most common method for controlling robotic arms, on the other hand, is still based on manually crafted scanning tables [29]. Inverse kinematic analysis is the accessibility of the determined end effector to the specified position within the arm parameters via the fixed reference axis set. Additionally, in inverse kinematic computations, analysis ought to be done on how many different configurations of accessibility are done. The geometric approach was used to analyze the inverse kinematic of the medical robot arm (figure 3).

Figure 3: Geometric approach of robot arm

15

$$|O_2O_5| = \sqrt{P_x^2 + P_y^2 + P_z^2} \qquad (14)$$

$$\theta_1 = tan^{-1}(P_x, P_y) \qquad (15)$$

$$|O_2B| = d = \sqrt{P_x^2 + P_y^2} \qquad (16)$$

Assume

$$|O_3O_4| = u = a_3 + a_4 \; ; |O_2O_3| = a_2 \qquad (17)$$

$$-cos(\theta_3) = \frac{(a_2)^2 + u^2}{2a_2u} \qquad (18)$$

$$|O_2C| = \sqrt{P_x^2 + P_y^2} - a_5c_{235} \qquad (19)$$

$$|O_2O_4|^2 = |O_2C|^2 + |O_4C|^2 \qquad (20)$$

$$|O_2O_4|^2 = |O_2O_3|^2 + |O_3O_4|^2 - 2|O_2O_3||O_3O_4|cos(180 - \theta_3) \qquad (21)$$

$$\theta_3 = tan^{-1}(S_3, C_3) \qquad (22)$$

$$\alpha = tan^{-1}(|O_4F|, |O_2F|) \qquad (23)$$

$$\beta = tan^{-1}(|O_4C|, |O_2C|) \qquad (24)$$

$$|O_4C| = P_z - a_1 + a_5S_{235} \qquad (25)$$

$$|O_2C| = a_1 + \sqrt{P_x^2 + P_y^2} - a_5C_{235} \qquad (26)$$

4. CONCLUSIONS

A robot arm with 360 degrees accessed any objects in the working space. The robot arm has the option of gripping any object with autonomous control. The system has an autonomous feature too. Motherboard use ATmega2560 microprocessor which stands out with its functional features.

The robot arm is manually controllable and the main purpose of the prototype robot arm is to use in specific tasks such as hazardous areas. It is a prototype study developed for use in rapid decision-making processes, especially in first aid recovery in industrial production enterprises or it is used in the hospital environment for reducing the workforce of hospital employees when transferring obese patients for such tasks.

It is extremely important in the development and popularization of open-source robots that especially no copyright issues and being cheaper compared to their industrial equivalents. The control software is open-source software that controls the 5 DoF robot arm and develops in the study. The working area was revealed by performing the kinematic analysis of the robot.

Thus, it was solved that the most important component required for the control of the robot arm used as auxiliary equipment for healthcare staffs. In the later stages of the study, it is aimed to add sound control and image enhancement process and develop control methods with software studies that will be

enriched with deep learning methods. For example, reading the barcode on the health worker with the voicemail message and leaving the desired material at the target point.

REFERENCES

[1] R. Gautam, A. Gedam, A Zade Mahawadiwar "A, Review on Development of Industrial Robotic Arm", International Research Journal of Engineering and Technology, Volume: 04 Issue: 03 | Mar -2017

[2] U. Schneider, JRD. Posada, et al ., "Automatic pose optimization for robotic processes", Robotics and Automation (ICRA), IEEE International Conference on. IEEE, 2015.

[3] A positioning paper by the International Federation of Robotics, Robots and the Workplace of the Future https://ifr.org/downloads/papers/IFR_Robots_and_the_Workplace_of_the_Future_Positioning_Paper.pdf

[4] NA. Radford, P. Strawser, K. Hambuchen, et al., Valkyrie: "NASA's first bipedal humanoid robot", J. Field Robot. 32, 397–419, DOI:10.1002/rob.21560, 2015

[5] J. Hurst, "Walk this way: to be useful around people, robots need to learn how to move like we do", IEEE Spectr 56, 30–51, DOI:10.1109/MSPEC. 2019.8651932, 2019

[6] G. Wagner, and H. Choset, "Subdimensional expansion for multirobot path planning. Artificial Intelligence", 219, 1–46. https://doi. org/10.1016/j.artint.2014.11.001, 2013

[7] M. Gharbi, J. Cortés, and T. Siméon, "Roadmap composition for multi-arm systems path planning". In: IEEE/RSJ international conference on intelligent robots and systems (pp. 2471–2476). https://doi.org/10.1109/IROS.2009.5354415, 2009

[8] T. Asfour, J. Schill, H. Peters, et al., "ARMAR-4: a 63 DOF torque controlled humanoid robot", in: Proceedings of the 13th IEEE-RAS International Conference on Humanoid Robots, Atlanta, USA, pp. 390–396, 2013

[9] J. Englsberger, A. Werner, C. Ott, et al., "Overview of the torque-controlled humanoid robot Toro", in: Proceedings of the 14th IEEE-RAS International Conference on Humanoid Robots, Madrid, ES, pp. 916–923, 2014

[10] RK. Reynolds, AP. Advincula, "Robot-assisted laparoscopic hysterectomy: technique and initial experience". Am J Surg 191:555–560, 2006

[11] TM. Beste, KH. Nelson, JA. Daucher "Total laparoscopic hysterectomy utilizing a robotic surgical system". J Soc Laparoendosc Surg 9:13–15, 2005

[12] C. Diaz-Arrastia, C. Jurnalov, G. Gomez, Townsend CJr "Laparoscopic hysterectomy using a computer-enhanced surgical robot." Surg Endoscopy 16:1271–1273, 2002

[13] GS. Guthart, J Jr. Salisbury "The intuitive telesurgery system: overview and application." In: Robotics and automation, Proceedings. ICRA '00. IEEE international conference on, vol. 1. pp 618–621, 2000

[14] HM. Yip, P. Li, D. Navarro-Alarcon, YH Liu, "Towards developing a robot assistant for uterus positioning during hysterectomy: system design and experiments"; Robotics and Biomimetics, 1:9 DOI 10.1186/s40638-014-0009-0, 2014

[15] https://github.com/BCN3D (access date: 01/12/2020)

[16] https://www.microchip.com/wwwproducts/en/ATmega2560 (access date: 01/12/2020)

[17] http://evrodekor34.ru/en/mks-gen-v-1-4-opisanie-podklyuchenie-elektroniki-k-plate-mks-gen-v1-4-podklyuchenie.html (access date: 01/12/2020)

[18] http://www.ribu.at/PDF/Tb6560.pdf (access date: 01/12/2020)

[19] http://www.cncbotto.com/controller.pdf (access date: 01/12/2020)

[20] https://www.makerguides.com/tb6560-stepper-motor-driver-arduino-tutorial/ (access date: 01/12/2020)

[21] http://www.t-es-t.hu/download/microchip/an907a.pdf (access date: 01/12/2020)

[22] A. Çelebi, A. Korkmaz, T. Yılmaz, H, Tosun, "3 Boyutlu Yazıcı ile 6 Eksenli Robot Kol Tasarım ve İmalatı", International Journal of 3D Printing Technologies and Digital Industru 3:3 269-278. 2019.

[23] S. Kucuk and Z. Bingul, "The Inverse kinematics solutions of industrial robot manipulators", IEEE Conferance on Mechatronics, pages 274-279, 2004

[24] J. Denavit and R.S. Hartenberg, "A kinematic Notation for Lower- Pair Mechanism Based on Matrices" ASME Journal of Applied Mechanics, 215-221, 1955

[25] SR. Kuo, YB. Yang, "A rigid-body-qualified plate theory for the nonlinear analysis of structures involving torsional actions" Eng Struct 47:2–15, 2013

[26] https://github.com/SurreyEARS/BCN3D-Moveo (access date: 01/12/2020)

[27] WL. Xiao, S. Henning, L. Torsten, et al., "Closed-form inverse kinematics of 6R milling robot with singularity avoidance" Prod Eng Devel 5:103–110, 2011

[28] Y. Wu, LH. Cheng GF Fan, et al. "Inverse kinematics solution and optimization of 6-DOF handling robot" Appl Mech Mater 635–637:1355–1359, 2014

[29] S. Guo, HW. Li, JC Ji, ZF. Ming, "Kinematic analysis and simulation of a new-type robot with special structure" Adv. Manuf. 2:295–302 DOI 10.1007/s40436-014-0094-x, 2014

Homotopy perturbation technique to solve nonlinear systems of Volterra integral equations of 1st kind

[1]Ahmed A. Mohammed Fawze ,**[2]Borhan F. Juma'a** ,and **[3]Waleed Al Hayani**

[1]Mathematics Department, College of Computer Science and mathematics, University of Mosul, Mosul, Iraq
[2]Department of Computer Science, College of Computer Science and Information Technology, University of Kirkuk, Iraq
[3] Mathematics Department, College of Computer Science and mathematics, University of Mosul, Mosul, Iraq

Corresponding author: 1Ahmed A. Mohammed Fawze (e-mail: aahmedamer68@uomosul.edu.iq).

ABSTRACT Integral equations are topics of major interest and can found in a wide range of engineering and industrial applications. The analytical solutions of the integral equations is restricted to few range of applications, but in a general most authors tend to approximate or numerical methods due to the advances in the numerical methods and techniques. In the present paper, the He 'perturbation method will be modified to solve Volterra integral equations(VIE). In the present paper, He's homotopy perturbation(HPM) with a proposed technique was developed to" solve system of" Volterra integral equations of 1st type". Three different test problems were solved using the proposed technique and their results gave the impression that it is efficient for dealing with the Volterra integral equations.

KEYWORDS: Integral equations, approximate techniques, homotopy perturbation method.

1. INTRODUCTION

Integral equations are topics of major interest and can found in a wide range of engineering and industrial applications. The analytical solutions of the integral equations is restricted to few range of applications, but in a general most authors tend to approximate or numerical methods due to the advances in the numerical methods and techniques. He in 1999 introduced the HMP. His method was applied by both researchers in the science and engineering fields for solving a wide range of linear and nonlinear problems. Between 2000 and 2004, the He's method had been modified to resolve different kinde of integral equations with miscellaneous Differences

 In the present paper,' the He's perturbation technique will be modified to solveVIE. In the current paper, the modified version of the perturbed homotopy method was developed to resolve the system of VIE of 1st kind having the following form:

$$\int_0^x \zeta_i(x,t)k_i(y_1(x),y_2(x),\dots\dots,y_n(x))dt = f_i(x) \tag{1}$$

In equation (1), $f_i(x)$ are prior recognized functions, $\zeta_i(x,t)$ are called Kernels, and $k_i(y_1(x),y_2(x),...,y_n(x))$.

Exact and The sacrificial solution of integral equ. is of great Relevance because it has wide significance implementation in scientific research." Many researchers" [1,10,32,33] have solved various types of integral equations by several technique. By making use of operational matrix with block-pulse functions [11-14], this type of equations had been solved. The system of VIE of the 1st kind had been solved by AD technique [15,30,34], also by making some modification on homotopy perturbation method [16,31] solved nonlinear integral equations. In 2010, Masouri introduced' numerical solution of VIE. of the 1st kind by introducing an expansion-iterative technique". In the present paper, He's homotopy perturbation with a proposed technique was developed to solve system of VIE. of 1st type. Three different test problems were solved using the proposed technique and their results

gave the impression that it is efficient for dealing with the VIE." treat An operator that is integral or differential such that ":

$$\ell(u) = 0 \tag{2}$$

accordingly to homotopy technique, we can construct a homotopy $v(r; \rho): \Omega \times [0,1] \to \Re$ and the domain Ω satisfies:

$$H(r; \rho) = (1 - \rho)F(v) + p\ell(v) = 0 \tag{3}$$

In equation (3), ρ is called embedding parameter.

The term $F(v)$ is known as 'functional operator with known solution u_0, which can be gained easily. obviously, we have:

$$H(v;0) = F(v) \tag{4}$$

And

$$H(v;1) = \ell(v) \tag{5}$$

We show that this process of changing the include 'parameter from zero to unit is just a process of mutable from solution'. This is known as deformation and also in topology and is called symmetry. Therefore, we may postulate that the solution to eq. (4) and (5) can be 'expressed as': $v = v_0 + \rho v_1 + \rho^2 v_2 + \dots$ (6)

Putting $\rho = 1$, we get the approximate solution of equation (1) as follows:

$$u = \lim_{n \to 1} v = v_0 + v_1 + v_2 + \cdots \tag{7}$$

"Let us consider the system of VIE of first kind. In the new proposed approach, we split $f_i(x)$ to infinite sums as follows":

$$f_i(x) = \sum_{j=0}^{\infty} K_{ij}(x), i = 1,2,3, \dots, n \tag{8}$$

Defining;

$$\varphi_i(x; \rho) = \sum_{}^{\infty} K_{ij}(x)\rho^j, i = 1,2,3, \dots, n \tag{9}$$

Where

$\rho \in [0,1]$ is an embedding parameter, now at $\rho = 0$, $\varphi_i(x;0) = K_{i0}$, and at $\rho = 1$ $\varphi_i(x;1) = f_i(x)$. Let us now construct the homotopy' $Y_i(x; \rho): \Re \times [0,1] \to \Re$ ', which satisfies the following eq.

$$Y_i(x; \rho) = \varphi_i(x; \rho) + \rho Y_i(x; \rho) - \rho \int_0^N c_i(x,t)g_i(Y_i(x; \rho))dt i = 1,2,3, \dots, n \tag{10}$$

Where
$$Y_i(x; \rho) = Y_1(x; \rho), Y_2(x; \rho), Y_3(x; \rho), \dots \dots, Y_n(x; \rho) \tag{11}$$

$$Y_i(x; \rho) = Y_{i0} + \rho Y_i + \rho^2 Y_{i2} + \cdots.$$

exchange Eq. (10) into Eq. (9), 'and equating the terms with equal powers of', we can obtain a series of linear eq. and solving them, we can get the approximate solutions. next,

"The proposed approach has been applied to obtain accurate solutions to some linear and nonlinear systems of the first-type integrated Volterra equations"

Definition 1-1:

Any functional equation in which the unknown function appears under the sign of integration is called" **integral equation"**.

The general form of non-linear integral equations may be written as follows:

$$\vartheta(\chi)\mu(\chi) = \zeta(\chi) + \lambda \int_a^{b(\chi)} \kappa(\chi,\tau,\mu(\tau))d\tau \qquad \chi\epsilon I = [a,b]$$

where the forcing function $\zeta(\chi)$ and the kernel function $\kappa(\chi,\tau,\mu(\tau))$ are prescribed while $\mu(\chi)$ is the unknown function to be determined. The parameter λ is often omitted; it is, however, of importance in certain theoretical investigations (e.g. stability) and in the eigenvalue problem.

Definition 1-2:

The IE (1-1) is called **LIE** if the kernel $(\chi,\tau,\mu(\tau)) = \kappa(\chi,\tau)\mu(\tau)$, i.e.

$$\vartheta(\chi)\mu(\chi) = \zeta(\chi) + \lambda \int_a^{b(\chi)} \kappa(\chi,\tau)\mu(\tau)d\tau \qquad \chi\epsilon I = [a,b]$$

otherwise it is called **non-linear.**

Definition 1-3:

The IE (1-1) is said to be an equation of the **first kind,** if $\vartheta(\chi) = 0$,i.e

$$\zeta(\chi) = \lambda \int_a^{b(\chi)} \kappa(\chi,\tau,\mu(\tau))d\tau$$

Definition 1-4:

The IE (1-1) is called **non-linear Volterra integral equation(NLVIE)** if $b(\chi) = \chi$, i.e

$$\mu(\chi) = \zeta(\chi) + \lambda \int_a^{\chi} \kappa(\chi,\tau,\mu(\tau))d\tau$$

Example

'Consider the system of linear VIE of 1st kind':

$$\int_0^x \left((1-x^2+t^2)y_i(t) - (2x-t)y_2(t)\right)dt = -\frac{1}{3}x^3 - \frac{2}{15}x^5 \tag{12}$$

$$\int_0^x \left((x+t^2)y_i(t) - (2+x-t)y_2(t)\right)dt = -x^2 - \frac{1}{6}x^3 + \frac{1}{3}x^4 + \frac{1}{5} \tag{13}$$

<div align="center">Having</div>

$$y_1(t) = x^2, y_2(t) = x$$

as the exact solutions.

In eq.(12) and (13):

$$f_1(x) = -\frac{1}{3}x^3 - \frac{2}{15}x^5$$

$$f_2(x) = -x^2 - \frac{1}{6}x^3 + \frac{1}{2}x^4 + \frac{1}{5}x^5$$

Now splitting $f_1(x)$ as:

$$f_1(x) = -\frac{1}{3}x^3 - \frac{2}{15}x^5 = \sum_{j=0}^{\infty} K_{1j}(x)$$

With

$$K_{10}(x) = x^2$$

$$K_{11}(x) = -x^2 - \frac{1}{3}x^3 - \frac{2}{15}x^5$$

$$K_{21}(x) = -x - x^2 - \frac{1}{6}x^3 + \frac{1}{3}x^4 + \frac{1}{5}x^5$$

$$K_{2j}(x) = 0, \ j > 1$$

Now construct the homotopy" $Y_1(x;\rho): \Re \times [0,1] \to \Re \ \& \ Y_2(x;\rho): \Re \times [0,1] \to \Re$ ", which satisfies the adjective equation:

$$Y_1(x;\rho) = \varphi_1(x;\rho) + \rho Y_1(x;\rho) - \rho \int_0^x \left((1 - x^2 + t^2)y_i(t) - (2x - t)y_2(t)\right)dt \tag{13}$$

$$Y_2(x;\rho) = \varphi_2(x;\rho) + \rho Y_2(x;\rho) - \rho \int \left((x + t^2)y_i(t) - (2 + x - t)y_2(t)\right)dt \tag{14}$$

$$\tag{15}$$

exchange "Eq. (11) into Eq. (14) and (15), and then collecting terms of same power of p", we get:

$$\rho^0: \begin{cases} Y_{10} = K_{10} \\ Y_{20} = K_{20} \end{cases} \tag{16}$$

$$\rho^1: \begin{cases} Y_{11} = K_{11} + Y_{10} - \int_0^x \left((1 - x^2 + t^2)y_i(t) - (2x - t)y_2(t)\right)dt \\ Y_{21} = K_{21} + Y_{20} - \int_0^x \left((x + t^2)y_i(t) - (2 + x - t)y_2(t)\right)dt \end{cases} \tag{17}$$

Knowing that

$$Y_{10} = x^2 \quad Y_{20} = x \tag{18}$$

$$Y_{11} = Y_{12} \dots \dots = 0; Y_{21} = Y_{22} \dots \dots = 0 \tag{19}$$

And

$$y_1(x) = x^2 \quad y_2(x) = x \tag{20}$$

Example

Let us consider the integral 1st kind of NOVIE system ':

$$\int_0^x \left(y_i(t) + (x - t)y_2(t)\right)dt = -\frac{3}{4} + \frac{x}{2} + \frac{1}{2}x^2 + \frac{1}{12}x^4 + e^x - \frac{1}{4}e^{2x} \tag{21}$$

$$\int_0^x \left(y_2(t) + (x - t)y_1(t)y_2(t)\right)dt = \frac{5}{4} + \frac{x}{2} + \frac{1}{2}x^2 + \frac{1}{12}x^4 - e^x - \frac{1}{4}e^{2x} \tag{22}$$

In these two equations; $y_i = x + e^x$ and $y_i = x - e^x$ represent the exact solutions.

In the present example:

$$f_1(x) = -\frac{3}{4} + \frac{x}{2} + \frac{1}{2}x^2 + \frac{1}{12}x^4 + e^x - \frac{1}{4}e^{2x}$$

$$f_2(x) = \frac{5}{4} + \frac{x}{2} + \frac{1}{2}x^2 + \frac{1}{12}x^4 - e^x - \frac{1}{4}e^{2x}$$

As had been occurred in the previous example, let us start by splitting functions and let us start by splitting $f_1(x)$ as follows:

$$f_1(x) = -\frac{3}{4} + \frac{x}{2} + \frac{1}{2}x^2 + \frac{1}{12}x^4 + e^x - \frac{1}{4}e^{2x} = \sum_{j=0}^{\infty} K_{1j}(x)$$

with

$$K_{10} = x + e^x$$

$$K_{11} = -\frac{3}{4} + \frac{x}{2} + \frac{1}{2}x^2 + \frac{1}{12}x^4 + e^x - \frac{1}{4}e^{2x}$$

$$K_{1j} = 0, j > 1$$

Similarly|

$$f_2(x) = \frac{5}{4} + \frac{x}{2} + \frac{1}{2}x^2 + \frac{1}{12}x^4 - e^x - \frac{1}{4}e^{2x} = \sum_{j=0}^{\infty} K_{2j}(x)$$

With

$$K_{10} = x - e^x$$

$$K_{21} = \frac{5}{4} + \frac{x}{2} + \frac{1}{2}x^2 + \frac{1}{12}x^4 - e^x - \frac{1}{4}e^{2x}$$

$$K_{2j} = 0, j > 1$$

Now construct the homotopy $Y_1(x; \rho): \Re \times [0,1] \to \Re$ & $Y_2(x; \rho): \Re \times [0,1] \to \Re$, which satisfies the adjective eq.:

$$Y_1(x; \rho) = \varphi_1(x; \rho) + \rho Y_1(x; \rho) - \rho \int_0^x \left(y_i(t; \rho) + (x - t)y_i(t; \rho)y_2(t; \rho) \right) dt \tag{22}$$

$$Y_2(x; \rho) = \varphi_2(x; \rho) + \rho Y_2(x; \rho) - \rho \int_0^x \left(y_2(t; \rho) + (x - t)y_1(t; \rho)y_2(t; \rho) \right) dt \tag{23}$$

Similarly|

$$f_2(x) = \frac{5}{4} + \frac{x}{2} + \frac{1}{2}x^2 + \frac{1}{12}x^4 - e^x - \frac{1}{4}e^{2x} = \sum_{j=0}^{\infty} K_{2j}(x) \tag{24}$$

With

$$K_{10} = x - e^x$$

$$K_{21} = \frac{5}{4} + \frac{x}{2} + \frac{1}{2}x^2 + \frac{1}{12}x^4 - e^x - \frac{1}{4}e^{2x}$$

$$K_{2j} = 0, j > 1$$

'exchange Eq. (11) into Eq. (23) and (24)', and then collecting terms of same power of p, we

$$\rho^0: \begin{cases} Y_{10} = K_{10} \\ Y_{20} = K_{20} \end{cases} \tag{25}$$

$$\rho^1: \begin{cases} Y_{11} = K_{11} + Y_{10} - \int_0^x \left(Y_{10}(t) + (x - t)Y_{10}(t)Y_{20}(t) \right) dt \\ Y_{21} = K_{21} + Y_{20} - \int^x \left(Y_{20}(t) + (x - t)Y_{10}(t)Y_{20}(t) \right) dt \end{cases} \tag{26}$$

(

$$Y_{10} = x + e^x$$
$$Y_{20} = x - e^x \tag{27}$$
$$Y_{11} = Y_{12} \ldots \ldots = 0; Y_{21} = Y_{22} \ldots \ldots = 0 \tag{28}$$

And

$$y_1(x) = x + e^x$$
$$y_2(x) = x - e^x \tag{29}$$

Let us consider the system of nonlinear VIE having $y_i(x) = x^2$ and $y_2(x) = x$ as the exact solutions

$$\int_0^x (1 - x^2 + t^2)(y_i(t) + y_2^3(t))dt = -\frac{1}{12}x^6 - \frac{2}{15}x^5 + \frac{1}{4}x^4 + \frac{1}{3}x^3 \tag{30}$$

$$\int_0^x (5 + x - t)(y_1^3(t) - y_2(t))dt = \frac{1}{56}x^8 + \frac{5}{7}x^7 - \frac{1}{6}x^3 - \frac{5}{2}x^2 \tag{31}$$

In the present example:

$$f_1(x) = -\frac{1}{12}x^6 - \frac{2}{15}x^5 + \frac{1}{4}x^4 + \frac{1}{3}x^3 \tag{32}$$

$$f_2(x) = \frac{1}{56}x^8 + \frac{5}{7}x^7 - \frac{1}{6}x^3 - \frac{5}{2}x^2 \tag{33}$$

As had been occurred in the previous example, let us start by splitting functions and let us start by splitting $f_1(x)$ as follows:

$$f_1(x) = -\frac{1}{12}x^6 - \frac{2}{15}x^5 + \frac{1}{4}x^4 + \frac{1}{3}x^3 = \sum_{j=0}^{\infty} K_{1j}(x) \tag{34}$$

With

$$K_{10} = x^2$$
$$K_{11} = -\frac{1}{12}x^6 - \frac{2}{15}x^5 + \frac{1}{4}x^4 + \frac{1}{3}x^3 - x^3 \tag{35}$$
$$K_{1j} = 0, j > 1$$

Similarly

$$f_2(x) = \frac{1}{56}x^8 + \frac{5}{7}x^7 - \frac{1}{6}x^3 - \frac{5}{2}x^2 = \sum_{j=0}^{\infty} K_{2j}(x) \tag{36}$$

With

$$K_{10} = x$$
$$K_{21} = \frac{1}{56}x^8 + \frac{5}{7}x^7 - \frac{1}{6}x^3 - \frac{5}{2}x^2 - x \tag{37}$$
$$K_{2j} = 0, j > 1$$

Now construct the homotopy

$Y_1(x; \rho): \Re \times [0,1] \to \Re \& Y_2(x; \rho): \Re \times [0,1] \to \Re$, which satisfies the

$$Y_1(x; \rho) = \varphi_1(x; \rho) + \rho Y_1(x; \rho) - \rho \int_0^x (1 - x^2 + t^2)(y_i(t; \rho) + y_2^3(t; \rho))dt \tag{37}$$
$$Y_2(x; \rho) = \varphi_2(x; \rho) + \rho Y_2(x; \rho) - \rho \int (5 + x - t)(y_1^3(t; \rho) - y_2(t; \rho))dt \tag{38}$$

Substituting Equation (11) into Equations (38) and (39), and then collecting terms of same power of p, we get:

$$\rho^0 : \begin{cases} Y_{10} = K_{10} \\ Y_{20} = K_{20} \end{cases}$$

<div align="right">(39)</div>
<div align="right">(40)</div>

$$\rho^1 : \begin{cases} Y_{11} = K_{11} + Y_{10} - \int_0^x (1 - x^2 + t^2)\big(Y_{10}(t) + Y_{20}^3(t)\big)dt \\ Y_{21} = K_{21} + Y_{20} - \int_0^x (5 + x - t)\big(Y_{10}^3(t) - Y_{20}(t)\big)dt \end{cases}$$

<div align="right">(41)</div>
<div align="right">(42)</div>

With

$$Y_{10} = x^2$$
$$Y_{20} = x$$
$$Y_{11} = Y_{12} \ldots \ldots = 0; Y_{21} = Y_{22} \ldots . = 0 \tag{43}$$

And
$$y_1(x) = x^2$$
$$y_2(x) = x \tag{44}$$

2. CONCLUSIONS

Drawing on HPM, an analytical approach has been developed to solve the Volterra Type I integrated system of equations." When evaluating the examples", we noted that the proposed process is unpretentious in computation and highly effective in both linear and nonlinear situations. In addition, in most cases, 'it gives accurate solutions at a first rough estimation.

REFERENCES

[1] Armand A, Gouyandeh Z (2014). Numerical solution of the system of Volterra integral equations of the first kind. Int. J. Ind. Math. 6:1.

[2] Babolian E, Masouri Z (2008). Direct method to solve Volterra integral equation of the first kind using operational matrix with block-pulse functions. J. Comput. Appl. Math. 220:51-57.

[3] Biazar J, Babolian E, Islam R (2003). Solution of a system of Volterra integral equations of the first kind by Adomian method. Appl. Math. Comput. 139:249-258.

[4] Biazar J, Eslami M (2010a). Analytic solution for Telegraph equation by differential transforms method. Physics Letters A 374:2904-2906

[5] Biazar J, Eslami M (2010b). Differential transform method for quadratic Riccati differential equation. Intl. J. Nonlinear Sci. 9(4):444-447.

[6] Biazar J, Eslami M (2010c). Differential transform method for systems of Volterra integral equations of the first kind. Nonl. Sci. Lett. A, 1(2):173-181.

[7] Biazar J, Eslami M (2011). Differential transform method for nonlinear fractional gas dynamics equation. Intl. J. Physical Sci. 6(5):12031206.

[8] Biazar J, Eslami M, Aminikhah H (2009). Application of homotopy perturbation method for systems of Volterra integral equations of the first kind. Chaos, Solitons and Fractals 42:3020-3026.

[9] Biazar J, Eslami M, Ghazvini H (2008). Exact solutions for systems of Volterra integral equations of the first kind by homotopy perturbation method. Appl. Math. Sci. 2(54):2691-2697.

[10] Biazar J, Eslami M, Islam MR (2012). Differential transform method for special systems of integral equations. J. King Saud UniversityScience 24(3):211-24.

[11] Biazar J, Ghazvini H, Eslami M (2009). He's homotopy perturbation method for systems of integro-differential equations. Chaos, Solitons Fractals 39:1253-1258.

[12] Biazar J, Mostafa E (2011a). Differential transform method for systems of Volterra integral equations of the second kind and comparison with homotopy perturbation method. Int. J. Phy. Sci. 6(5):1207-1212.

[13] Biazar J, Mostafa E (2011b). A new homotopy perturbation method for solving systems of partial differential equations. Comput. Math. Appl. 62:225-234.

[14] Eslami M (2014a). New homotopy perturbation method for a special kind of Volterra integral equations in two-dimensional space. Comput. Math. Modeling 25(1).

[15] Eslami M (2014b). An efficient method for solving fractional partial differential equations. Thai J. Math. 12(3):601-611.

[16] Eslami M, Mirzazadeh M (2014). Study of convergence of Homotopy perturbation method for two-dimensional linear Volterra integral equations of the first kind. Int. J. Comput. Sci. Math. 5(1):72-80.

[17] Ghorbani A, Saberi-Nadjafi J (2008). Exact solutions for nonlinear integral equations by a modified homotopy perturbation method. Comput. Math. Appl. 56(4):1032-1039.

[18] Golbabai A, Keramati B (2008). Modified homotopy perturbation method for solving Fredholm integral equations, Chaos. Solitons and Fractals 37:1528-1537.

[19] He JH (1999). Comparison of homotopy perturbation method and homotopy analysis method. Appl. Math. Comput. 156(2):527-539.

[20] He JH (2000). A coupling method of homotopy technique and perturbation technique for nonlinear problems. Intl. J. Non-Linear Mech. 35(1):37-43. He JH (2003). A simple perturbation approach to Blasius equation. Appl. Math. Comput. 140:217-222.

[21] Maleknejad K, Najafi E (2001). Numerical solution of nonlinear volterra integral equations using the idea of quasilinearization, Commun Nonlinear Sci Numer Simulat 16:93-100.

[22] Maleknejad K, Shahrezaee M (2004). Using Runge–Kutta method for numerical solution of the system of Volterra integral equation. Appl. Math. Comput. 149:399-410.

[23] Maleknejad K, Sohrabi S, Rostami Y (2007). Numerical solution of nonlinear Volterra integral equations of the second kind by using Chebyshev polynomials. Appl. Math. Comput. 188:123-128.

[24] Masouri Z, Babolian E, Hatamzadeh-Varmazyar S (2010). An expansion–iterative method for numerically solving Volterra integral equation of the first kind. Comput. Math. Appl. 59:1491-1499.

[25] Ngarasta N, Rodoumta K, Sosso H (2009). The decomposition method applied to systems of linear Volterra integral equations of the first kind. Kybernetes. 38(3/4):606-614.

[26] Odibat ZM (2008). Differential transform method for solving Volterra integral equation with separable kernels. Math. Comput. Modelling 48:1144-1149.

[27] Rabbani M, Maleknejad K, Aghazadeh N (2007). Numerical computational solution of the Volterra integral equations system of the second kind by using an expansion method. Appl. Math. Comput. 187:1143-1146

[28] Saeedi L, Tari A, Masuleh SH (2013). Numerical solution of some nonlinear Volterra integral equations of the first kind. Applicat. Appl. Math. 8(1).

[29] Tahmasbi A, Fard OS (2008). Numerical solution of linear Volterra integral equations system of the second kind. Appl. Math. Comput. 201:547-552.

[30] K. K. Abbo, Y. A. Laylani, and H. M. Khudhur, "Proposed new Scaled conjugate gradient algorithm for Unconstrained Optimization," *Int. J. Enhanc. Res. Sci. Technol. Eng.*, vol. 5, no. 7, 2016.

[31] K. K. Abbo and H. M. Khudhur, "New A hybrid Hestenes-Stiefel and Dai-Yuan conjugate gradient algorithms for unconstrained optimization," *Tikrit J. Pure Sci.*, vol. 21, no. 1, pp. 118–123, 2015.

[32] K. K. ABBO, Y. A. Laylani, and H. M. Khudhur, "A NEW SPECTRAL CONJUGATE GRADIENT ALGORITHM FOR UNCONSTRAINED OPTIMIZATION," *Int. J. Math. Comput. Appl. Res.*, vol. 8, pp. 1–9, 2018, [Online]. Available: www.tjprc.org.

[33] K. K. Abbo and H. M. Khudhur, "New A hybrid conjugate gradient Fletcher-Reeves and Polak-Ribiere algorithm for unconstrained optimization," *Tikrit J. Pure Sci.*, vol. 21, no. 1, pp. 124–129, 2015.

[34] H. N. Jabbar, K. K. Abbo, and H. M. Khudhur, "Four--Term Conjugate Gradient (CG) Method Based on Pure Conjugacy Condition for Unconstrained Optimization," kirkuk Univ. J. Sci. Stud., vol. 13, no. 2, pp. 101–113, 2018.

Investigation of Innovations in Solar Generator Systems

[1]Bekir Çırak 🆔 , **[2]Arife Pınar** 🆔

[1] Department of Mechanical Engineering, Karamanoglu Mehmetbey University, TURKEY
[2] Mechanical Engineering Department Graduate Student, Karamanoğlu Mehmetbey University, TURKEY

Corresponding author: Bekir Çırak (bcirak@kmu.com)

ABSTRACT The sun, which has the most energy on earth, is also the world's main energy source. All fossil fuels are indirect solar energy. Many renewable energy sources, such as winds and ocean waves, are indirectly related to sunlight. Therefore, collecting energy directly from the sun is a practical way. Photovoltaic (PV) based solar panels currently on the market have also been used commercially for some time. PV modules started with the production of hard silicon solar cells in history. For this reason, flat solar panels have technological advantages. In this study, information about the details of the solar cells produced and in the design phase are compiled from the literature. In addition, scientific, theoretical and applied information about the elements of solar generators was collected. It was presented for the use of researchers. Future formations and innovations are mentioned about solar collectors and its elements.

KEYWORDS: Solar Energy, Generator, Photosensitive, Renewable Energy, Innovation.

1. INTRODUCTION

News about climate change is getting more annoying day by day, and knowing that climate change should not happen is the sad part of this situation. Energy sources that did not harm the world, did not change its atmosphere, and could provide energy for people, started to live with the creation of the universe. The energy sector will undergo significant changes in the future. The percentage of renewable energies will increase, especially in wind, solar and hydroelectric use. All of these variable resources will present challenges to national networks [1]. Fossil fuels were fairly simple to extract and use, and the Earth hadn't gotten much into solar work from them to charging technique, so they remained cheap without being expensive. Therefore, it continued to be forgotten for many years without coming together with advanced technology. Oil-free power generation is an engineering feat for mankind, between 2000 and 2010 was a period of powerful innovation for solar technology. Research projects or commercial initiatives have emerged that aim to make solar energy a power generation source. While some studies are financially supported by state institutions, entrepreneurs and industrialists do not provide this support in places where there is no state support. It is predicted that the efforts, reputation and financial instruments of scientists, engineers, entrepreneurs and philanthropists will have an important position in the future. It is among these predictions and claims that businesses and machines will operate with renewable energy, most of which is solar energy. In addition to the work these innovators do to move us in this direction, the efforts of politicians,

educators and other visionaries who strive to prevent the worst climate consequences are also noteworthy. There are three major categories of solar technology;

1. Photovoltaic systems convert sunlight directly into electricity. In silicon conductors, they generate electricity using light-absorbing materials. Electrons in these materials are released by solar energy and pass through an electrical circuit to power electrical devices.

2. They are used for solar heating and cooling systems.

3. Concentrated solar technology concentrates the energy from the sun using mirrors to drive conventional electricity-generating steam turbines or engines [2].
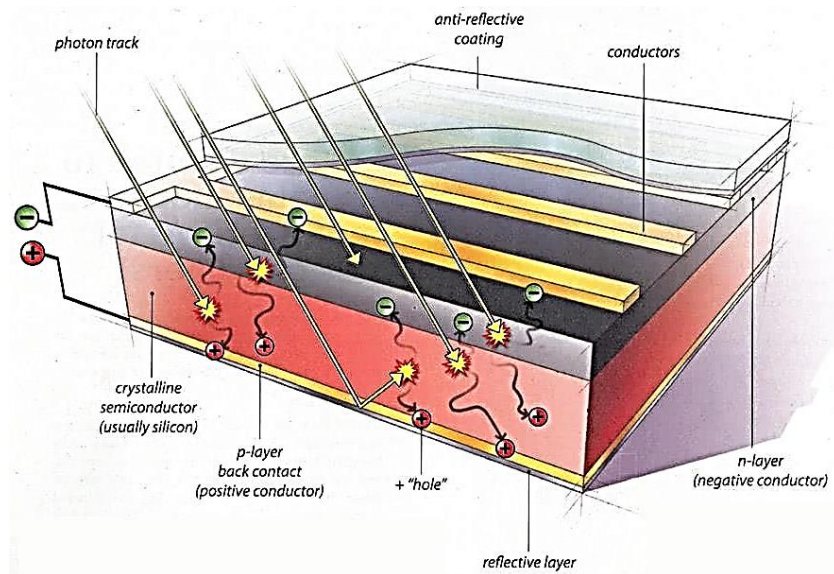
In this article, research examples on photovoltaic cells, batteries, wireless solar transmission and Concentrated solar energy are presented.

2. PHOTOVOLTAIC CELLS (PV)

Photovoltaic cells convert photons in sunlight into electricity. The PV effect was observed by Alexandre Edmund Becquerel in 1839, and in 1954 Bell Labs invented the first usable solar PV device. The solar cell's conductive layer is made of a refined silicon crystal, similar to the material in computer chips. These cells have an efficiency rate of about 20 percent for converting sunlight into electrical energy. The rigid solar panel consists of a group of solar cells all integrated in a single plane [3]. PV cell research aims to reduce the cost of solar cells and increase their efficiency. It is important to use widely available materials in common innovations.

Another research parameter is to improve reliability: toxic or flammable materials should be avoided. Silicon-based solar PV manufacturing involves using the same materials as the microelectronics industry. Commonly used perovskite solar cells contain well-known toxin lead, methyl ammonium lead iodide is the preferred material for such solar cells. A very small amount and very low probability of leakage in a solar cell. However, researchers are investigating the health risks and dangers of lead-based perovskite materials [4].

PV modules contain recyclable and reusable materials such as glass, aluminum and semiconductor materials. In today's technology, recycling of thin film and silicon modules takes place. The parts of the PV module are shown in Figure 1 [5] .

Figure 1. Elements of PV modules [5]

3. SPHERICAL SUN POWER GENERATOR

A Protatip solar generator will produce twice as much efficiency than a traditional solar panel despite having a much smaller surface area. With the hybrid collector, it is used to convert daily electricity and thermal energy at the same time [3].

The modular collector system, developed by German architect Andre Broessel for his company Rawlemon, it recharges and stores energy during the daytime and can even collect energy from moonlight and ambient light at night. Rawlemon website states, "Using a high efficiency multi-junction cell, the cell surface was reduced to 1% in optimum conditions compared to the same power output as a silicon cell. The system produces twice the efficiency of a normal panel Also, a smaller cell area has a lower carbon footprint as its production requires less valuable semiconductor or other building materials. "Multi-junction cells made of multiple materials react to multiple wavelengths of light and some of the energy to be lost can be captured and transformed. Multi-junction cells can only work with concentrator systems [6] Spherical lens systems are shown in Figure 2.

Figure 2. Spherical Lens Systems [6]

4. POLYMER SOLAR CELLS

Polymers are a technology inherent in products such as polystyrene plastic. When heated, the thermoplastic polymer softens and can be converted into semi-finished products such as films and sheets. Polymer solar cells have desirable lighter weight and flexibility properties. However, they require a technical extra process steps and coating technologies. The researchers added a textured substrate model that provides a thin, uniform light-absorbing layer to flexible, lightweight polymers. This textured substrate pattern remains thin in flat-topped protrusions that are less than a millionth of a meter. With this layer, productivity increased by 20 percent [7].
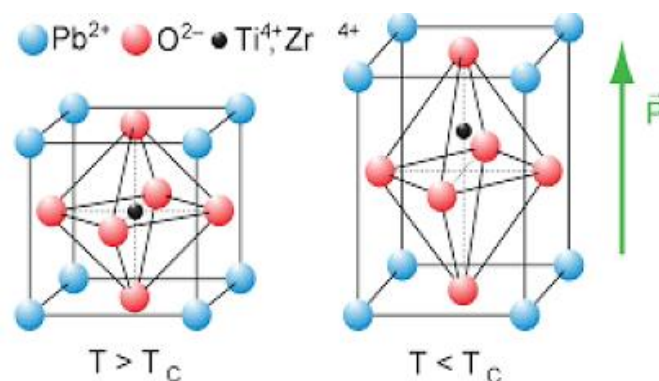
5. ULTRA SHORT PULSE LASER SCRİBİNG

Polymers are a technology inherent in products such as polystyrene plastic. When heated, the thermoplastic polymer softens and can be converted into semi-finished products such as films and sheets. Polymer solar cells have desirable lighter weight and flexibility properties. However, they require a technical extra process steps and coating technologies. The researchers added a textured substrate model that provides a thin, uniform light-absorbing layer to flexible, lightweight polymers. This textured substrate pattern remains thin in flat-topped protrusions that are less than a millionth of a meter. With this layer, productivity increased by 20 percent [8].

6. FDT LİGHT HARVESTİNG FİLM

One of the successful and preferred solar cells is light-harvesting films produced from perovskite materials with the same type of crystal structure as calcium titanium oxide ($CaTiO_3$). Perovskite-based solar cells use expensive hole-carrying materials to move the positive charges created when light hits the perovskite film. Scientists have now made a molecularly engineered hole-carrying material called FDT. By comparison, they claimed that FDT was easy to synthesize and its cost would be almost 1/5 of the available materials."FDT is able to keep the solar cell's efficiency above 20% [8]. The Light Harvesting Film of crystallization and its chemical structures are shown in Figure 3.

Figure 3. Light Harvesting Film of Crystalling and Chemical Structure [9]

7. TANDEM PEROVSKİTE SİLİCON CELLS

Researchers believe perovskites pave the way for high-efficiency, low-cost solar cells. Perovskites are easily synthesized and absorb light in the blue region of the spectrum, contain silicon that can absorb long wavelength red and near infrared light. Scientists found that a new tandem solar cell containing monolithic perovskite and silicon produced electricity with an efficiency of 18 percent.Although this is not the maximum solar cell efficiency rate, they believe it may be sufficient for industry studies. Many parts of the world have established production facilities for silicon cells. Perovskite layers can significantly increase the productivity level. To achieve this, production techniques need to be supported by only a few production steps FG [10]. The crystal and natural structure of Light Harvesting Film is shown in Figure 4.

Figure 4. Light Harvesting Film of Crystalling and Natural Structure [10]

8. 3D PRİNTED SOLAR ENERGY TREES

Researchers at the VTT Technical Research Center in Finland developed some decorative prototypes thanks to advanced solar and 3D printing technologies and called them "energy harvest trees". Thanks to the small leaves, it can provide power to small household appliances and mobile devices by storing solar energy. Small leaves thrive indoors and outdoors, and can collect kinetic energy from the surrounding wind and temperature differences. The leaves of the tree are flexible organic solar cells and each individually has a power converter. The crates are 3D printed and wood-based bio-composites are used as raw materials. They are mass producible [11]. The crystal and natural structure of Light Harvesting Film is shown in Figure 5.

Figure 5. 3D Produce of Energy Harvesting Trees [11]

9. CERİA FOR SOLAR FUEL PRODUCTİON

Ceria or cerium oxide, which is the most common on earth, tends to exhale and exhale alternately as it warms or cools oxygen. It is considered a tool for generating fuel. A new prototype formulated by the researchers uses a quartz window to pass sunlight through a small gap in a cylinder filled with cerita. When water or carbon dioxide is pumped into the tank, hydrogen and / or carbon monoxide is formed. Hydrogen is used alone in hydrogen cells, and a synthetic fuel (syngas) is produced by mixing hydrogen and carbon monoxide. The resulting fuels are portable and can be used at any time. Researchers believe that improved insulation and smaller openings increase efficiency by up to 19%, making this a viable option [12]. Crystallized and atomic structures are shown in Figure 6.

Figure 6. Crystalling and Atomic Structure for Seria [12]

10. BATTERİES and STORAGE

The biggest problem of generating electricity from renewable sources is that it is not continuous. Photovoltaic cells can generate energy from sunlight. However, in order for this energy to be available at night or in cloudy weather, they must be integrated with some kind of storage mechanism. The users of the energy they obtain with photo voltaic can use it if they need energy when the sun is not shining.

Until now, energy storage batteries have been based on lead-acid chemistry, which is polluting, short-lived and unreliable. Lithium is an alternative to lead as it is the lightest of all metals and has great electrochemical potential. Lithium ions are advanced technology produced in the market. Various battery chemistry studies are close to this technology. Battery storage systems are among the researches that are being conducted all over the world [13].

The aim of all these developments is to produce cheaper, safer storage capacity for renewable resources with longer life and operational capacity [14].

The first period in lithium battery history. The success of lithium iodine battery, lithium potential and somehow clearing the way the development of a capable range of new batteries it was to meet the demands of various, diverse applications. [15]

10.1 Tesla: Lithium İon

Tesla began manufacturing the lithium-ion Powerwall battery at a large factory near a lithium mine in Nevada. Powerwall is a household battery that partners with solar panels to provide the stored power for use at night or during outages. With the battery, a house can achieve net and zero energy ratio, meaning it can generate as much energy as it consumes while connected to the electricity grid during periods of high demand. Each Powerwall has an energy storage capacity of 7 kWh and multiple batteries can be installed together to meet larger energy needs. This capacity can be increased up to 10 kWh [16].

Tesla presented its first demo home system batteries in 2015 and 2016. It also offers a 100 kWh battery for utility scale use. Tesla aims to generate 10,000 Powerpacks and 1Gw of electricity. Tesla CEO stated that with 160 million Powerpacks it will enable the entire USA to transition to renewable energy and with 900 million Powerpacks the whole world will make the transition.The lithium ion powerwall battery is shown in Figure 7 [17].

Figure 7. Lithium-İon Powerwall Battery [16]

10.2 Sonnenbatterie: Lithium İon

Sonnenbatterie, a German company, also entered the US market in 2015. German scientists discovered the lithium-ion Sonnenbatterie in 2015. For their storage systems, Sony Fortelion uses lithium-ion batteries and they claim that they can be used for up to 10,000 charge cycles [18], [19].

10.3 Aquion Energy: Aqueous Sodium İon

Cradle to Cradle Material Health certified The world's first battery works with salt water and other commonly available materials and stores enough solar or wind energy to run a home for eight hours. A dishwasher or small refrigerator size, the Aqueous Hybrid Ion (AHI) battery can be easily placed in grid and micro grid positions. Aquion Energy has full scale production in many countries of the world [16]. The Aqueous Hybrid Ion (AHI) battery is shown in Figure 8 [20].

Figure 8. Aqueous Hybrid Ion (AHI) Battery [20]

10.4 Ambri: Liquid Metal

The Ambri battery has different weights and melting points and allows the two metals to work together by separating them with a layer of salt. Electric currents heat metals to 700^0 Celsius ($1{,}292^0$Fahrenheit), pushing electrons into molten salt. It has been observed that Ambri, which has negative test results, attaches importance to the production of gaskets that keep the liquid electrodes closed and steel boxes that must be sealed airtight with long-life materials. In other words, in the production facility of Ambri, he is still looking for a solution to the sealing problem [21],[22].

10.5 Seeo: Dry Lithium

Seeo, the founder of Silicon Valley, is developing a battery for the electrolyte that uses a solid dry polymer that is less flammable than a liquid one. It uses lithium for the anode and a new material that can store more energy for the cathode in the manufacture of the battery. Seeo has been producing these batteries for testing purposes for some time now. Recently, it was seen that German auto parts manufacturer Bosch bought dry lithium production [18]. The dry lithium battery is shown in Figure 9 [23].

Figure 9. Dry Lithium Battery [23]

10.6 In Research: Lithium-Air

The potential of lithium air is due to the fact that it uses lithium and oxygen, two very mild elements that react to form the lithium peroxide product. In October 2015, the University of Cambridge announced several changes in Science that would start mass production of lithium air cells, but some major transactions are still in progress. The team plans to create a highly porous electrode using sheets of graphene as thick as a single atom. Another modification was to replace lithium peroxide with lithium hydroxide (LiOH) [24].

11. IN RESEARCH: POLYMER BASED REDOX FLOW

The battery developed by German scientists consists of organic polymers and a harmless salt solution. The electrodes of this redox flow battery are made of dissolved form materials. It is not made of solid materials such as metals or metal salts. Electrolyte solutions are stored in two tanks that form the negative and positive terminal of the battery. Polymer solutions are transferred with the help of pumps to an electrochemical cell where the polymers are electrochemically reduced or oxidized, through which the battery is charged or discharged [25].

12. IN RESEARCH: THERMO CHEMİCAL TECHNOLOGY

In solar energy conversion, it uses photovoltaic cells to convert beam energy into electricity. Researchers at the Massachusetts Institute of Technology (MIT) used a method to capture and release solar energy via thermochemical fuel. Thermochemical technology captures solar energy and stores it in the form of heat in its chemical molecules, conserving heat energy to be converted and used later. In fact, the product can be called "rechargeable heat cell". In early experiments, a rare chemical element, ruthenium, was used at a controllable cost. Researchers are examining the exact working mechanism of the ruthenium to find another chemical element more readily found in nature or to synthesize the material in the laboratory [26].

13. WİRELESS SOLAR TRANSMİSSİON

Much greater efficiency in converting sunlight into electricity could be achieved if the energy conversion is done in space, not on earth. Although the field of climate researchers is to determine the parameter values of the energy flow to the earth, it is a fact that about 29% of the solar energy reaching the top of the atmosphere is reflected back into space by clouds and atmospheric particles. Bright ground like sea ice and snow is big in this projection [27].

Therefore, Japanese scientists conducted a successful ground demonstration test for wireless power transmission. They also revealed that long-range wireless power transmission technology is an applicable technology. It will play a role at the center of space-based solar energy (SBSP) systems, which are expected to be among the new technologies. A solar cell orbiting 36,000 kilometers above the earth could potentially generate power, which could then be sent to earth via a microwave without

being connected to wires. Researchers think that this new technology could be an effective energy source in solving both environmental and energy problems in the world. Their goal is to transmit energy from solar panels in orbit by 2030 [28], [29]. Space Based Solar Energy Systems (SBSP) are shown in Figure 10.

Figure 10. Space Based Solar Power Systems (SBSP) [29]

The Space Solar Energy Exploration Research and Technology program (SERT) was created by NASA and then aimed to convert sunlight into electricity using an inflatable photovoltaic gossamer structure with condenser lenses or solar heat engines. Included China and India in the NASA Space Solar Program. This collaboration is space collaboration talking about space-based solar energy. China announced that scientists are planning the construction of a solar power plant 36,000 kilometers above the ground. If realized, it will be the largest space project ever [30].

14. CONCENTRATİNG SOLAR POWER (CSP)

Solar power plants use mirrors to collect sunlight and store the collected energy as heat. Many CSP systems, such as natural gas, coal, and nuclear power plants, also require access to water for cooling. All require little water to collect and wash mirror surfaces, but some plants can use wet, dry, and hybrid cooling techniques to maximize water savings. CSP facilities must have access to an electricity grid to distribute the harvested power nnn [26]. In 2016, the largest concentrated solar power (CSP) power plant in the world went into operation.

In Morocco, it is planned that, in addition to hydro and wind, about half of its electricity will be supplied from renewable sources by the end of 2020. It is the location of a complex of four interconnected solar mega-power plants. The project is an important step in the use targets for the country. It makes deserts free from energy. When construction is complete, the plant will have the capacity to generate 580 MW of electricity, enough to power one million homes.

In the first phase, 500,000 parabolic shaped solar mirrors are used in 800 rows with a generation capacity of 160 MW. Each parabolic mirror is 12 meters high and focuses on a steel pipeline that provides heat transfer, a synthetic thermal oil that is heated to 393ºC as it bends along the gutter before being wound on a heat engine. There it is mixed with water to create steam that spins energy-

generating turbines. The heat tank contains melted sand that can store heat energy for three hours. Morocco imports 94% of its energy as fossil fuel from abroad. Concentrated Solar Power (CSP) facility is shown in Figure 11 [14].

Figure 11. Concentrated Solar Power (CSP) Plant [14]

15. HYDROGEN PRODUCTION and USE

The main technique used in this study is green hydrogen. It is used to denote low-carbon hydrogen produced from renewable energy sources. It is also used to denote blue hydrogen. Low carbon hydrogen produced from non-renewable sources, typically natural gas and coal, brown. He talks about the use of carbon capture and storage technology. In this study, clean hydrogen was used as an element.

It is derived from low carbon hydrogen, green, blue, and nuclear energy. The term hydrogen was not used in majority in this study, but nuclear derived hydrogen has been explicitly mentioned. CO_2-free hydrogen is often used in Japan denotes low carbon hydrogen but it is not included in this study.

The distinction between hydrogen and hydrogen based fuels is discussed in this article. Hydrogen, a form of synthetic fuel, for greater clarity, hydrogen and other synthetic fuels were used separately. The molecular formula of hydrogen is (H_2). Synthetic fuels; It has been used for synthetic fuels other than molecular hydrogen. Power-to-X (PtX) is used for this. In this study, to produce hydrogen and hydrogen-based synthetic fuels, the study has been continued by taking the entire usage process of electricity as a reference [31].

Low carbon investment options; Energy-related CO2 emissions have increased by 1% per year in the last decade. As health shock and oil slump could suppress emissions in 2020, a recovery it would revive the long-term trend.

The Transformation Energy Scenario offers a climate-safe path instead [31].

16. DRILLING THERMAL ENERGY STORAGE APPLICATIONS and ON-SITE THERMAL RESPONSE TEST - THE CASE of TURKEY and THE SITUATION IN TURKEY

Underground thermal energy storage system; (UTES) is reliable, sustainable and energy efficient. Building cooling, heating technology and is used in industrial processes all over the world. In this article, various UTES applications in the last 20 years are mentioned. UTES, a technology for energy storage; used in ground, aquifers or underground pools. Inside, heat waste from solar energy is stored in different ways and is. It is used for heating. A similar method is followed in the cooling process. This method has been applied in many applications. It has been developed within the framework of the International [32].

16.1 History of Thermal Intervention

Thermal conductivity; It is found by the proper dimensioning of the ground and an underground covering an energy well. This system is a thermal energy system. Effective in-situ heat to estimate the conductivity of the system; The thermal response of a well is found by measuring the ground. Field tests are done with a mobile thermal response test (TRT) apparatus (Figure 1) [32].

Figure 12. In-situ TRT apparatus [32]

17. CONCLUSİON

Future energy plans depend on many factors. State leaders, scientists, and energy investors may not always agree on the best route. Low carbon investment options Energy-related CO2 emissions have increased by 1% per year in the last decade. As health shock and oil slump could suppress emissions in 2020, a recovery it would revive the long-term trend. The Transformation Energy Scenario offers a climate-safe route instead [33]. Fossil fuel energy is currently required to implement solar applications, and if the remaining oil and gas resources are not applied to their development, subsequent generations will be fed directly or roughly by sunlight before the industrial revolution. The pioneers whose work is described here will encounter both alternatives of the fossil fuel age. They will be exposed to more primitive means. This article aims to plant a seed of foresight in mind to see beyond the oil age. Technologies currently under development point to a time when there will be cleaner, cheaper and safer ways to generate heat and cooling, provide water, and empower people with more power than humans for daily work. [2], [7].

REFERENCES

[1] International Energy Agency, "Implementing Agreement for a Programme of Research and Development on Energy Conservation through Energy Storage", Strategic Plan 2016 – 2021.

[2] Anonim, SEIA, "The Solar Energy Industries Association", [Çevrimiçi]. Available at: https://www.seia.org/initiatives/about-solar-energy .

[3] M. Mercure, "Photovoltaic (Pv) Cells", 2021. [Çevrimiçi]. Available at: https://solarindustrymag.com/.

[4] Anonim, "PV Cell Research". [Çevrimiçi]. Available at: http://materials.com/.

[5] Anonim, "Photovoltaic", 2017. [Çevrimiçi]. Available at: http://www.renewableenergyfocus.com/category/60/photovoltaics-pv/.

[6] Rawlemon, "Spherical Solar Power Generators", 2019. [Çevrimiçi]. Available at: https://rawlemon.com/spherical-solar-power-generators.

[7] Anonim, "Alternative Energy", [Çevrimiçi]. Available at: https://www.alternative-energy-news.info/best-use-of-polymer-solar-cells/.

[8] E. Venere, "'Ultra fast laser "engraving" Technique to Reduce Costs and Increase the Efficiency of Solar Cells'", 2011. [Çevrimiçi]. Available at: https://www.purdue.edu/.

[9] Anonim, "Solar Cell", [Çevrimiçi]. Available at: https://actu.epfl.ch/news/cheaper-solar-cells-with-202-efficiency/ .

[10] Anonim, "Silikon Solar Cell", [Çevrimiçi]. Available at: https://cleantechnica.com/2015/11/12/tandem-perovskite-silicon-solar-cell-efficiency-record-broken/.

[11] Anonim, "3D Printed Solar Energy Trees", [Çevrimiçi]. Available at: http://www.alternative-energy-news.info/3d-printed-solar-energy-trees/.

[12] Anonim, "Alternative Energy", [Çevrimiçi]. Available at: https://www.alternative-energy-news.info/ceria-mimics-plant-life/.

[13] A. Sherden, "Explained: The tesla powerwall and what it means for Australia's energy market", 2016. [Çevrimiçi]. Available at: https://batteryuniversity.com/.

[14] Anonim, "US agency reaches 'holy grail' of battery storage sought by Elon Musk and Gates", 2016. [Çevrimiçi]. Available at: https://www.theguardian.com/international.

[15] B. Scrosati, "History of Lithium Batteries", Journal of Solid-State Electrochemistry, 15(7-8), 1623-1630, 2011.

[16] Anonim, "Tesla: Lithium İon". [Çevrimiçi]. Available at: https:// www.teslamotors.com

[17] Anonim, "No Title", 2015. [Çevrimiçi]. Available at: https://www.emirates247.com/search7.117?sd&qlithium+ion&author&dr&dfdt .

[18] W. Steel, "Tesla's schröder moving back to sonnenbatterie". [Çevrimiçi]. Available at: https://cleantechnica.com/.

[19] R. Ossenbrink, "Sonnenbatterie begins product development in the USA". [Çevrimiçi]. Available at: https://sunwindenergy.com/.

[20] Anonim, [Çevrimiçi]. Available at: http://www.aquionenergy.com/energy-storage-technology .

[21] Anonim, [Çevrimiçi]. Available at: https://www.bloomberg.com/searchquery=Ambri: liquid-metal

[22] M. LaMonica, "Ambri is better grid battery", 2013. [Çevrimiçi]. Available at: https://www.technologyreview.com/ .

[23] K. Fehrenbacher, "Why bosch is buying silicon valley battery startup seeo", 2015. [Çevrimiçi]. Available at: https://fortune.com/.

[24] Anonim, "New breakthrough in lithium-oxygen battery technology". [Çevrimiçi]. Available at: https://iflscience.com/.

[25] F.-S.-U. Jena, "Synthetic batteries for the energy revolution", 2015. [Çevrimiçi]. Available at: https://www.sciencedaily.com/.

[26] D. L. Chandler, "Catching The Sun's Heat", 2010. [Çevrimiçi]. Available at: http://www.alternative-energy-news.info/ .

[27] Anonim, [Çevrimiçi]. Available at: https://earthobservatory.nasa.gov/features/EnergyBalance/page4.php .

[28] Anonim, "Expanding the potential for new industrial applications", 2015. [Çevrimiçi]. Available at: https://www.mhi.com/news/1503121879.html .

[29] E. Ackerman, "Japan demoes wireless power transmission for space-based solar farms", 2015. [Çevrimiçi]. Available at: https://spectrum.ieee.org/energywise/green-tech/solar/japan-demoes-wireless-power-transmission-for-spacebased-solar-farms.

[30] Anonim, "Space solar energy exploration research and technology program (SERT)". [Çevrimiçi]. Available at: http://www.xinhuanet.com/english/home.htm.

[31] Frontier Economics, International Aspects of a Power-to-X Roadmap: A Report Prepared for the World Energy Council, Germany (https://www.frontier-economics.com/media/2642/frontier-int-ptx-roadmap-stc-12-10-18-final-report.pdf), 2018

[32] U. Stritih, D. Rajver, B.Turgut and H. Paksoy, & quot; Borehole thermal energy storage applications and in-situ thermal response test-Example from Turkey and situation in Slovenia", Journal of Mechanical Engineering, 50:6, 328-340, 2004.

[33] IRENA, International Renewable Energy Agency. Global Renewables Outlook: Energy Transformation, Abu Dhabi, 2020-2050.

Voltage Profile Improvement using DSTATCOM Based on Artificial Intelligence Techniques

Fouad Zaro

Electrical Engineering Department, Palestine Polytechnic University, Hebron, PALESTINE

Corresponding author: Fouad Zaro (e-mail: fzaro@ppu.edu).

ABSTRACT The demand for electric power has recently increased as a result of an increase in residential and industrial facilities that may contain sensitive nonlinear loads that require high power quality (PQ) on the distribution system to avoid malfunction. The improvement of voltage profiles with appropriate voltage harmonic distortion is a major PQ problem. It should be monitored to keep it within reasonable limits. The distribution static synchronous compensator (DSTATCOM) is used with an established control strategy to boost the voltage profile. DSTATCOM control is developed in this study using artificial intelligence (AI) and the artificial neural network (ANN), which is focused on optimum values found by particle swarm optimization (PSO). The simulation results demonstrated that DSTATCOM's proposed control strategy for improving the voltage profile on the distribution system is superior and stable. The MATLAB/Simulink software package was used to validate the performance.

KEYWORDS: Artificial Neural Networks, DSTATCOM, PI controller, Power Quality, Voltage Profile

1. INTRODUCTION

The rapid rise in electrical power consumption has resulted in the increased usage of renewable energy sources (RES) and distributed generation (DG) in the electrical grid. When new energy resources enter the grid and different types of loads, such as nonlinear loads, different difficulties develop in current, voltage, and/or frequency, causing instrument error and malfunction, which is referred to as power quality (PQ) difficulties [1].

Several researches have been conducted on PQ difficulties, utilizing the benefits of major advancements in power electronics technology, resulting in a network transition from traditional to smart. PQ can also be defined as electrical limitations that allow a piece of equipment to work properly and at a high level of performance. Poor PQ, according to these definitions, has a negative impact on the electrical network's dependability and stability, as well as sensitive loads linked to the distribution bus's end user. PQ is concerned with three key factors: voltage, current, and frequency, all of which should be kept within acceptable ranges [2].

PQ issues in the network are produced by a variety of factors, including the connection of nonlinear loads, such as big motors in industrial applications, power electronics devices, switching capacitor banks, and the addition of new electrical resources to the grid. Indeed, these disturbances have an impact on the distribution system's performance and operation, as well as sensitive equipment. The smart grid (SG) technology opens up a lot of possibilities for resolving PQ issues. Flexible alternating current transmission systems (FACTS), a family of power electronics technologies, complement SG systems and offers answers to PQ issues. The distribution static synchronous compensator (DSTATCOM),

which is a shunt device attached to the distribution bus, is one application of the FACTs family. Voltage var control is one of the most important parts of a power system, hence voltage var optimization (VVO) is the key SG application that improves power system security and efficiency. Artificial intelligence (AI) development is now playing a major role in the optimization of power system concerns, particularly in SG [3].

Several PQ studies have focused on enhancing and increasing the electrical grid's dependability and stability. These studies focus on challenges such as voltage profile improvement in power systems, imbalance circumstances in systems caused by unbalanced loading and load change, symmetrical and unsymmetrical failures, actual and reactive power losses due to harmonic distortion, and low power factor (PF). To address these PQ difficulties, several FACTs devices are used. Different DSTATCOM control techniques are susceptible to non-ideal supply conditions and load fluctuations, necessitating careful controller design tuning for each individual insulator. In addition, the cost of the system rises as a result of the employment of specialized equipment like the LCL filter. Other DSTATCOM control systems in the literature required extensive control facilities and controllers, as well as supplemental components like active filters. In addition, the controller may require additional delay time due to the analogue-to-digital conversion [4-5].

On the other hand, new proposed control techniques for DSTATCOM have been implemented, such as an adaline-based algorithm and a direct method that is based primarily on output voltage position and magnitude control. Although these strategies have been confirmed as effective for managing DSTATCOM, they are more complicated and costly than previous procedures. DSTATCOM analyzes and implements various control techniques using various mathematical theories and physical models. The dynamic system equations are simplified using instantaneous power theory, rotating reference frame (dq0), stationary reference frame, instantaneous reactive power (IRP), and Park's transformation [6-7].

FACTS devices and smart controls that are compatible with renewable energy supplies have been the subject of extensive research. Existing RES and DGs in the electricity system provide unique issues, particularly when these resources have a high penetration rate. To meet these issues, SG technology is required to manage the grid's power flow. The power created or absorbed by FACTS devices, as well as the power created or absorbed by RES. Using SG technology improves the power system's dependability and stability, even when the number of RES connected to the distribution bus is high. Many studies have been completed on optimization approaches for various PQ concerns in power systems. A comparison of meta-heuristic approaches such as GA, PSO, differential evolution (DE), harmony search (HS), and seeker optimization algorithm (SOA) is included in these papers [8-13]. As a result of the literature research, there are significant obstacles in utilizing AI techniques to tune DSTATCOM's PI controller. This paper proposes the use of ANNs as a strategy for tweaking the DSTATCOM controller, whose controller constants are best determined using PSO [14-17].

42

This work offers an AI methodology, specifically PSO and ANN, that is employed in the DSTATCOM design controller to improve the voltage profile on distribution electrical power systems. DSTATCOM settings and design are introduced in part II. The proposed system's mathematical model is described in Section III. The created AI methodologies and proposed optimization strategy for developing the developed controller for DSTATCOM are discussed in detail in section IV. The methodology is presented in Section V, which includes a description of a real-world distribution system as a case study. Section VI shows the simulation findings for the proposed scenarios in this study, as well as a full discussion of all outcomes for voltage events such as sag and swell. Finally, section VII summarizes the suggested approach's performance, efficiency, and superiority.

2. DSTATCOM CONFIGURATION AND DESIGN

The circuit diagram of the equivalent model of DSTATCOM is shown in Fig.1 [6].
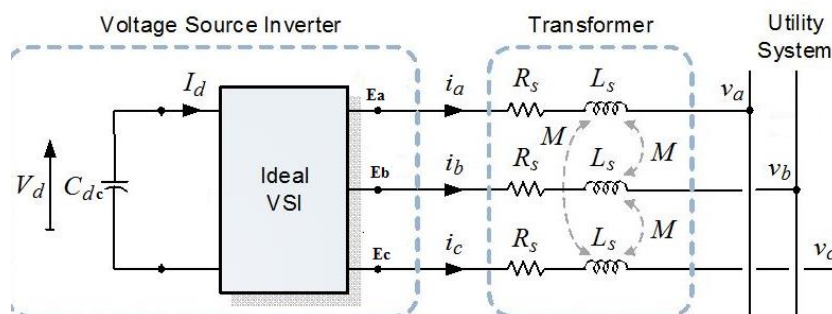

Figure 1. Equivalent model of DSTATCOM.

Where:

R_s and L_s: are DSTATCOM transformer resistance and inductance respectively.

E_{abc}: are converter AC side phase voltages.

V_{abc}: are the ac system side phase voltages.

i_{abc}: are phase currents.

I_d: is capacitor current.

C_{dc}: is dc capacitor value.

The voltage source converter (VSC) is the main electrical component of DSTATCOM, transforms dc to ac voltage. In this investigation, the following forms of VSC were used:

1. A gate turn-off thyristor is utilized to create a square wave 48-step voltage waveform of four three-level inverters; however, specific interconnection transformers are utilized to eliminate harmonics from the output voltage waveform.

2. This inverter uses isolated gate bipolar transistors and employs PWM to convert DC input voltage to AC output voltage sinusoidal waveform (IGBT).

DSTATCOM's operation is divided into three modes:

1. Mode 1: when the output voltage Vout amplitude is larger than the utility bus voltage Vac, current flows from the converter to the AC side of the power system via reactance, and the DSTATCOM injects reactive power into the AC side of the power system.

2. Mode 2: when the voltage at the utility bus is less than the amplitude of Vout, current flows from the AC side of the power system to the converter, and DSTATCOM absorbs reactive power from the AC power system.

3. Mode 3: there is no reactive power exchange between DSTATCOM and the power system when the output voltage V_{out} amplitude equals the voltage amplitude at the AC side of the power system; in this situation, DSTATCOM is in a floating condition.

The PI controller is used to control the function of DSTATCOM to inject the required reactive current to the load. Figure 2 shows the simplified scheme of control strategy of DSTATCOM [8].
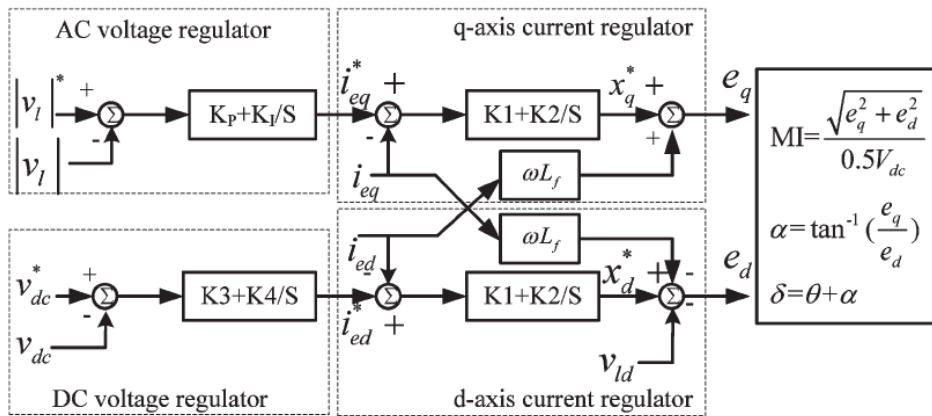

Figure 2. Control strategy scheme of DSTATCOM

PWM controls the output voltages for VSI based on the modulation index (MI) and phase angle between the inverter voltage and line voltage. DSTATCOM's PI controller is in charge of generating/absorbing the desired reactive power at the power system's common coupling point [11]. The purpose of this type of control is to keep the voltage magnitude at PCC constant throughout system disruptions. The controller input in Figure 3 is an error signal, which is the difference between the RMS reference voltage (1pu) and the RMS value of the observed terminal voltage. To minimize the error to zero, the PI controller processes the error signal and generates the needed drive angle [15].
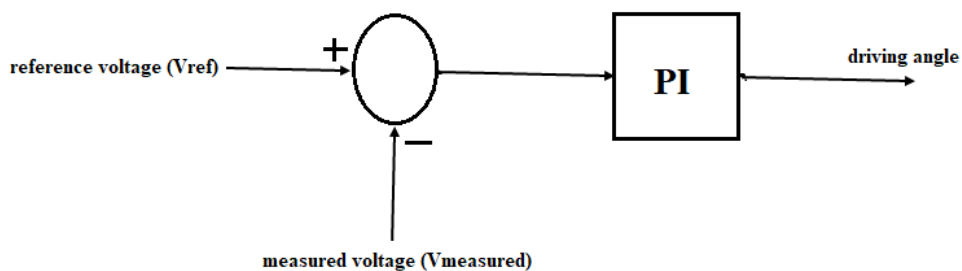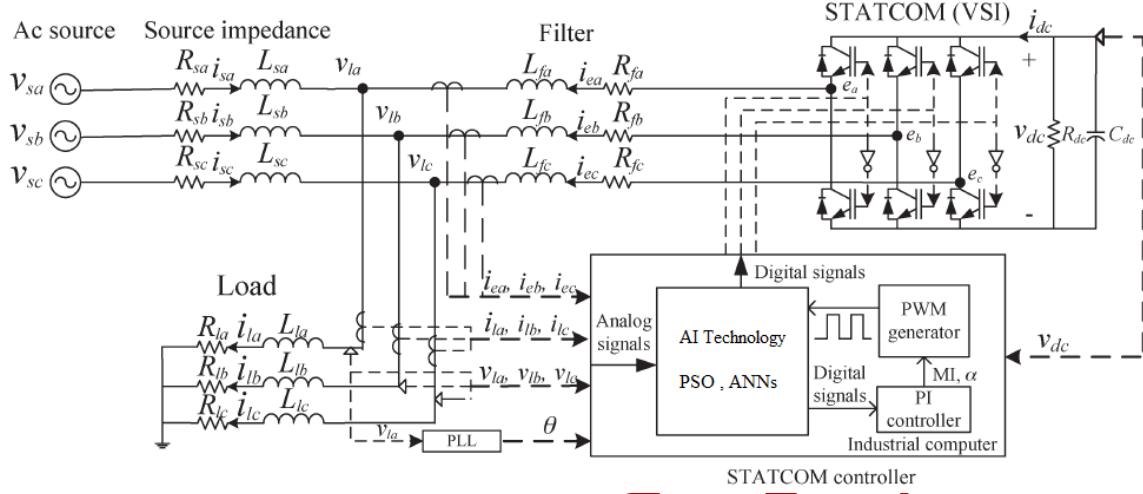

Figure 3. Direct PI control of DSTATCOM

3. MATHEMATICAL MODEL OF PROPOSED DSTATCOM

Because DSTATCOM has a nonlinear operation structure, the control strategy of DSTATCOM is studied using simplified mathematical formulas. The configuration parameters of DSTATCOM connected to the power grid are illustrated in Figure 4 [8].

Figure 4. DSTATCOM Configuration connected on power system.

The inverter voltage magnitude Vc and the angle difference between the bus voltage and the inverter output voltage govern the actual and reactive power of DSTATCOM. Equations (1) and (2), respectively, explain DSTATCOM's active and reactive power compensation [10]:

$$P = \frac{V_{Pcc}V_c \sin\alpha}{X} \tag{1}$$

$$Q = \frac{V_{Pcc}(V_{Pcc} - V_c \cos\alpha)}{X} \tag{2}$$

Where:

P: active Power.

Q: reactive Power

Vc: inverter Voltage

V_{Pcc}: voltage at the point of common coupling

α: angle of V_{pcc} with respect to V_c

X: reactance of the branch and the transformer.

DSTATCOM's controller is based on the system's dynamic equations and is constructed with the assumption that the system is linear [8].

4. DSTATCOM DESIGN

The equations of the mathematical model of the specified system [11] to be used to calculate DSTATCOM components, which include:

4.1 DESIGN DC BUS VOLTAGE

Current compensation can be determined using the following equation if the voltage DC link is sufficient.

$$V_{dc\,min} > \sqrt{2}V_{L-L(rms)} = \sqrt{2}\,\sqrt{3}V_{L-N(rms)} \tag{3}$$

4.2 DESIGN DC BUS CAPACITOR

The C_{dc} can be calculated using the energy conservation principle:

$$\frac{1}{2}C_{dc}[V_{dc}{}^2 - V_{dc1}{}^2] = 3\,k\,a\,V\,I\,t \tag{4}$$

Where:

V_{dc}: is the reference DC bus Voltage

V_{dc1}: is the minimum level of the DC bus voltage

a: is the over loading factor

V: is the phase voltage

I: is the phase current

t: is the time for which the DC bus voltage is to be recovered

k: factor for variation of energy during dynamics

4.3 DESIGN AC INTERFACING INDUCTOR

The following equation determines which filter to use based on the ripple current icr-pp, switching frequency fs, and DC bus voltage V dc:

$$L_f = \frac{\sqrt{3}\,m\,V_{dc}}{12\,a\,f_s\,i_{cr-pp}} \tag{5}$$

Where *m* is modulation index.

4.4 DESIGN PASSIVE HIGH PASS RIPPLE FILTERS

To eliminate the high frequency noise from the voltage waveform at PCC in the power system the high pass filter is needed to do that, it could be calculated by the following formula:

$$R_r C_r = \frac{T_s}{10} \tag{6}$$

46

5. ARTIFICIAL INTELLIGENCE AND OPTIMIZATION TECHNIQUES

5.1 PARTICLE SWARM OPTIMIZATION

PSO is a social and cooperative behavior-inspired heuristic search optimization approach. The approach is linked to the primary components. The first is influenced by personal behavior (P_{best}), while the second is influenced by social experience (G_{best}). These two pieces [14] determine how the particle's position in search space is updated. The technique's fundamental equations are as follows:

$$V_{i,j}^{k+1} = w \times V_{i,j}^{k} + c_1 \times r_1 \times \left(P_{besti,j}^{k} - X_{i,j}^{k}\right)(15) + c_2 \times r_2 \times \left(G_{besti,j}^{k} - X_{i,j}^{k}\right) \tag{7}$$

$$X_{i,j}^{k+1} = X_{i,j}^{k} + V_{i,j}^{k+1} \tag{8}$$

Where $P_{besti,j}^{k}$ represent personal best jth component of ith individual, whereas G_{bestj}^{k} represents jth component of the best individual of population up to iteration k. The PSO search mechanism is multidimensional search space. The considered steps of PSO technique is shown in the following flowchart.
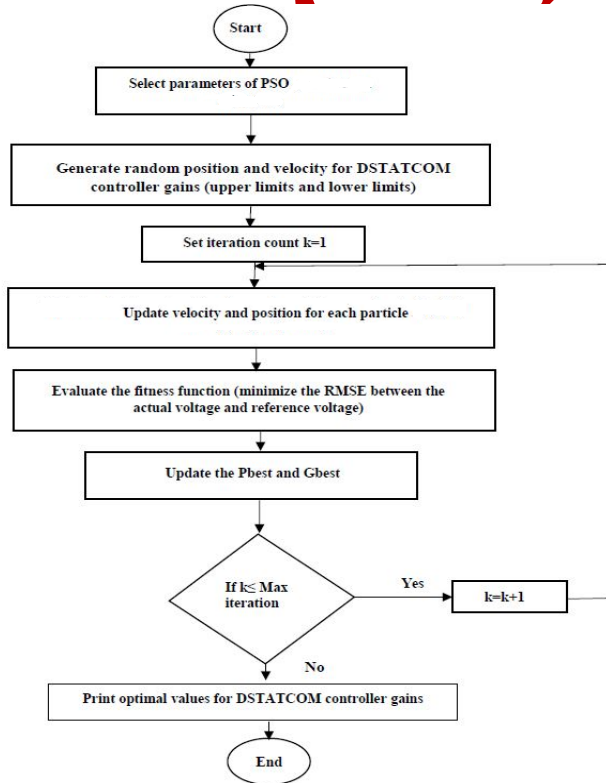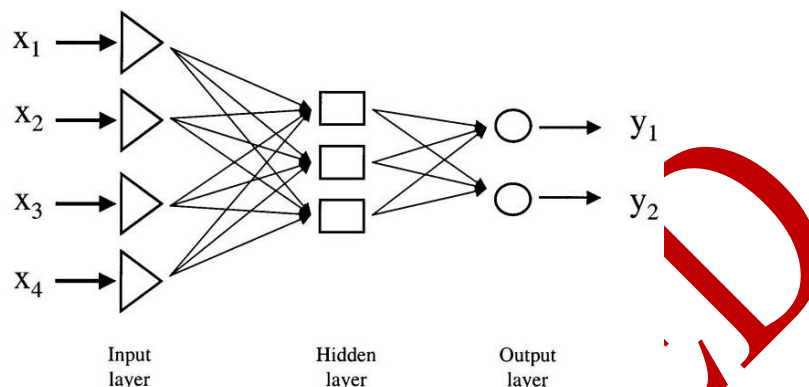

Figure 5. Flowchart of PSO algorithm

5.2 ARTIFICIAL NEURAL NETWORKS (ANNS)

forward-thinking DSTATCOM's controller is tuned in real time based on the voltage level of the distribution bus using ANN. The basic design of an ANN feed forward is shown in Figure 6, which consists of three layers: input, hidden, and output. Each layer's node (neurons) is linked to the following

layer's node. The number of input nodes in the input layer corresponds to the number of system inputs, and the number of output nodes in the output layer corresponds to the number of system outputs. The number of hidden nodes in the middle layer is usually equal to the sum of the system's input and output nodes. Because both overfitting and underfitting have an impact on training results [15-16], the number of hidden nodes is critical.

Figure 6. Basic neural network structure

The training procedure of the feed forward ANN used in this study is according to the mean square error of output criterion, which can be defined by
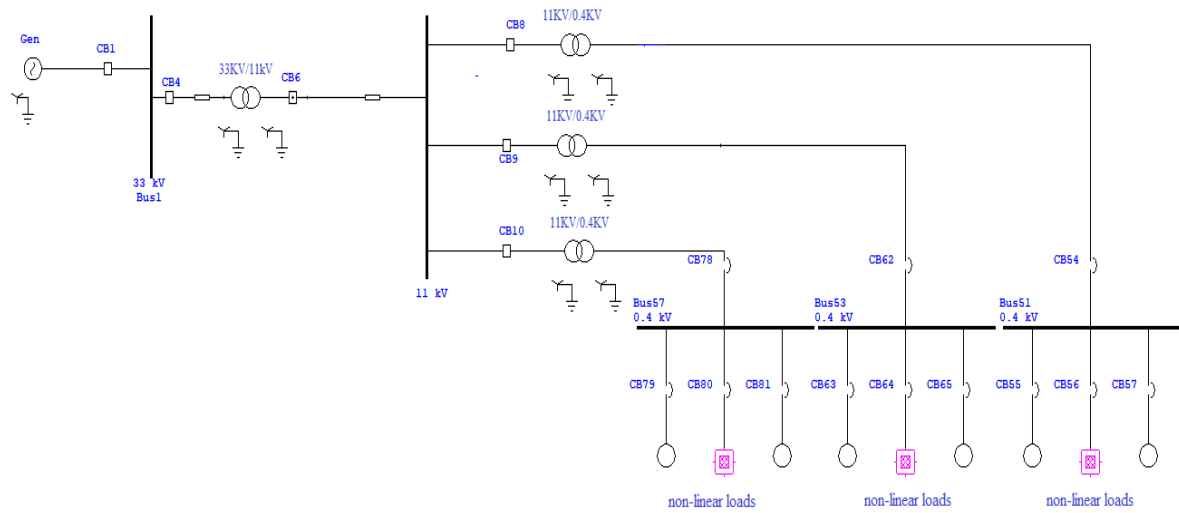
$$J = \sum_{1}^{N} e(i)^2 \qquad (9)$$

Where N is the output neurons number, and $e(i)$ is instantaneous error between the actual and estimated value of the output.

The value of each neuron in the output layer (y_j) is given in terms of the input values x_i as shown in the following equation

$$y_j = \tanh(\sum w_{ij} x_i + b_j) \qquad (10)$$

6. CASE STUDY

The work is tested on a live network using data provided by the Jerusalem District Electricity Company (JDECO). The network is for the West Bank's Abu Mashaal zone. Due to industrial nonlinear loads, the voltage on this network falls below the standard level (11kV) on the distribution bus. Figure 7 shows a single line diagram of the provided radial network.

Figure 7. Single line diagram for radial network

Description of the system configuration is summarized in Table 1

Table 1. Description of proposed distribution feeder

Parameter	Value
3 phase ac source	V_{rm}=11kV, f=50Hz
Line impedance	L_s=3.851mH, R_s=0.211Ω
Distribution transformers	33kV/11kV, 11kV/0.4kV

The rated load connected on the end user of distribution system is 1MVA, Table 2 summarize the calculation values of DSTATCOM configuration.

Table 2. Values of DSTATCOM configuration

Parameter	Value
I_{rms}	1443.3A
V_{dc}	15556.3V
C_{dc}	16.665mF
L_f	31.42μH
C_r	1.8mF
R_r	0.0027Ω

7. TUNING DSTATCOM CONTROLLER USING ANNS AND PSO

7.1 EMPLOY PSO FOR OPTIMUM VALUE OF CONTROLLER

The PSO method is used to determine the best DSTACOM controller gains (Vac regulator, Vdc regulator, and current regulator and PLL regulator). The goal is to reduce the root mean square error (RMSE) between the actual measured voltage and the reference voltage as much as possible (1pu). The following equations represent the objective function:

$$RMSE = (\frac{1}{n} \sum_{i=1}^{n} (V_i - V_{ref})^2)^{\frac{1}{2}} \qquad (11)$$

$$J = \min[RMSE] \qquad (12)$$

Where:

J: fitness function

$RMSE$: Root mean square error

V_i: actual voltage

V_{ref}: reference voltage(1pu)

n: number of samples

7.2 EMPLOY ANNS FOR CONTROL DSTATCOM

The usage of ANN as an AI tool for controlling DSTATCOM is presented. Because ANN controllers can proficiently learn the unknown continuously altering environment and act accordingly, they have become a wide subject of interest among researchers in a wide range of fields. The PSO findings were analyzed for a wide range of sag and swell occurrences (0.7-1.3), with roughly 70% of these data being used as a data foundation for the ANN training procedure. The output of the ANNs are then used to control DSTATCOM in real time. The ANN learning process is created in MATLAB with the help of the toolbox neural network.

In order to apply the ANNs algorithm for learning and discover the optimum optimal value of controllers gains according to disturbance voltage level, eight networks are defined in MATLAB code for this study, as shown in Table 4.

Table 3. Define networks in ANN algorithm

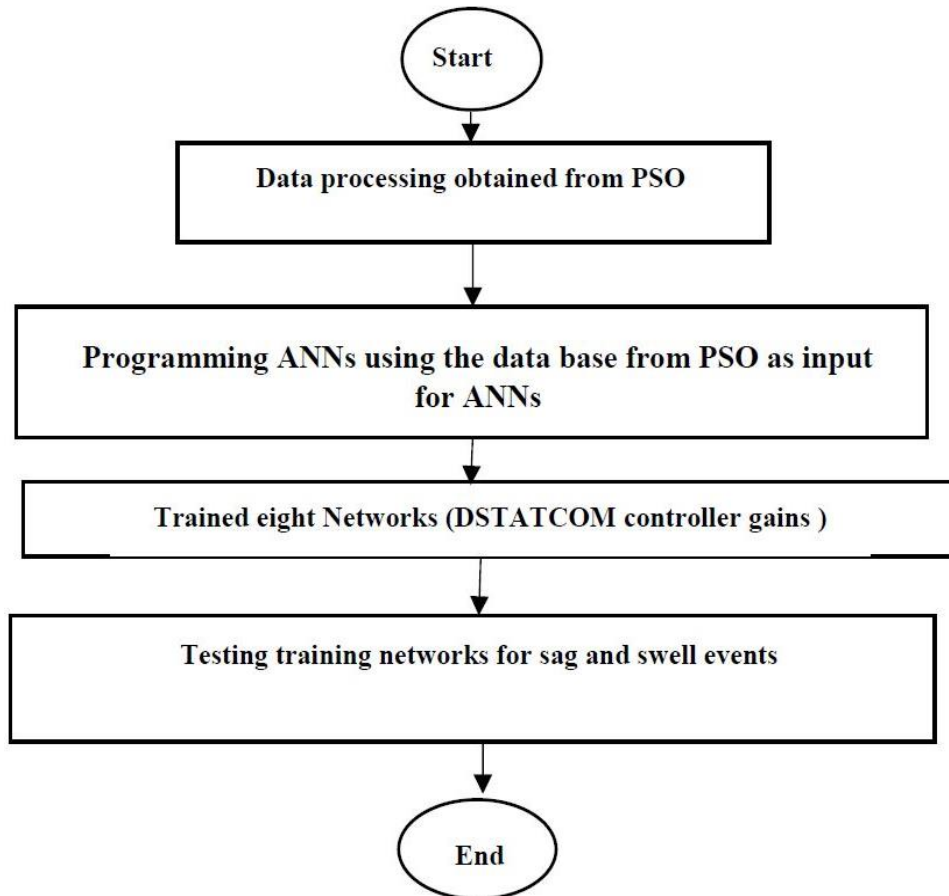| ANNs	Controller gain
Network1	$V_{ac}(k_p)$
Network2	$V_{ac}(k_i)$
Network3	$V_{dc}(k_p)$
Network4	$V_{dc}(k_i)$
Network5	$i(k_p)$
Network6	$i(k_i)$
Network7	$PLL(k_p)$
Network8	$PPL(k_i)$

7.3 DESIGNING AND PROGRAMMING ANNS

Generally, programming ANNs follow a number of systemic procedures:

- Collecting of data from the PSO: the values of k_p and k_i for each case of sag and swell events using PSO.
- Data reprocessing in this step the data is normalized.

- Building the network.
- Training the network.
- Testing the network by used the targets output in simulation model.

Figure 8 describes the Basic flowchart for designing ANN Model.

Figure 8. Basic flowchart for designing ANNs model

PSO is used as a tool to obtain the optimum values of controller gains. Then data processing is done and nearly 70% of these data is used to train eight networks that control DSTATCOM as mention in Table 4. Values for controller gains is applied to ANNs in training phase. ANN logarithm is used for practice the controller and select the gains constants according to activations elements. The controller constants are used as inputs to train the eight controller constants networks.
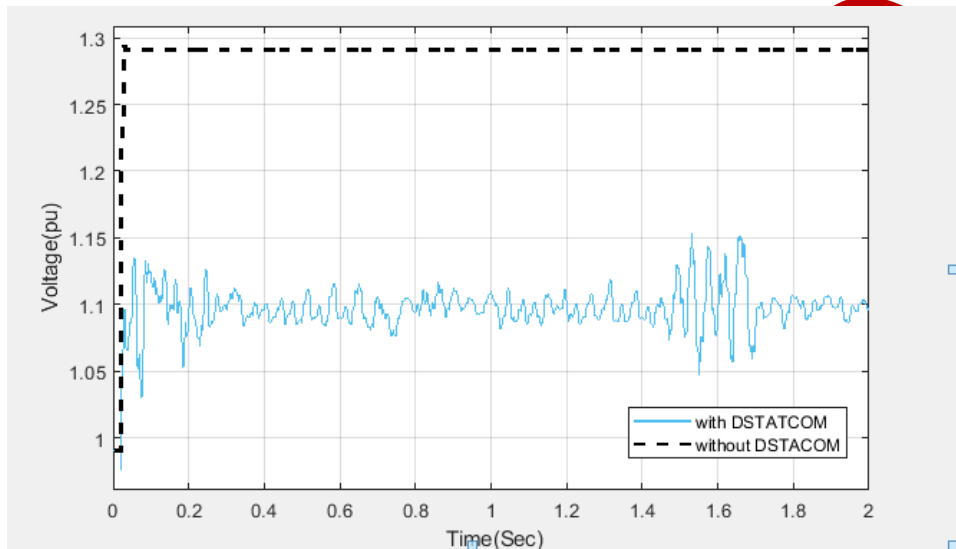
8. RESULTS DISCUSSION

The ANN logarithm is used to test the controller and choose its gains constants based on the activation's elements. Nearly 70% of the data obtained through PSO is used in the algorithm. The findings and controller gains for extreme swell and extreme sag using DSTATCOM's created controller are shown in Table 5.

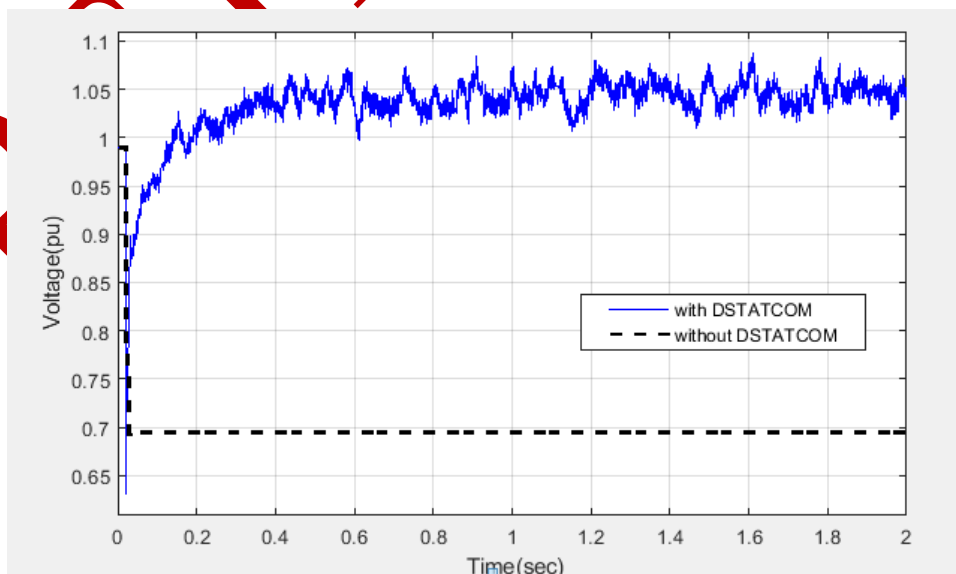**Table 5.** Voltage profile improvement using developed DSTATCOM controller

Event	Voltage profile improvement	THD%
Extreme swell (1.3pu)	1.02pu	3.26
Extreme sag (0.7pu)	1.07pu	9.23

The effect of DSTATCOM on enhancing the voltage profile of the system at the PCC during a voltage swell event with an acceptable range is shown in Figure 9.
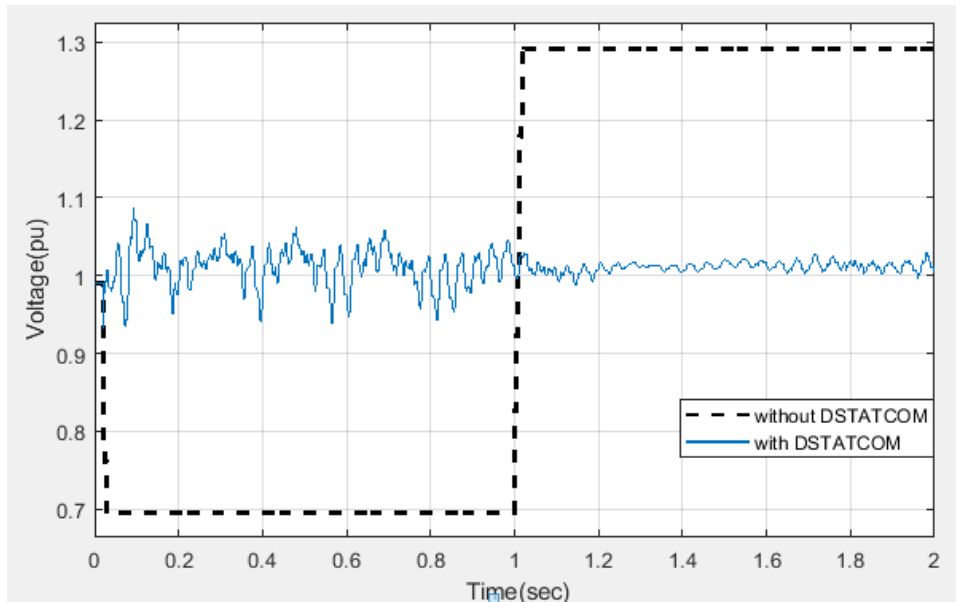

Figure 9. Effect of DSTATCOM on Voltage profile during extreme swell event.

DSTATCOM's effect on enhancing the voltage profile of the system at the PCC during a voltage sag event with an acceptable range is shown in Figure 10.
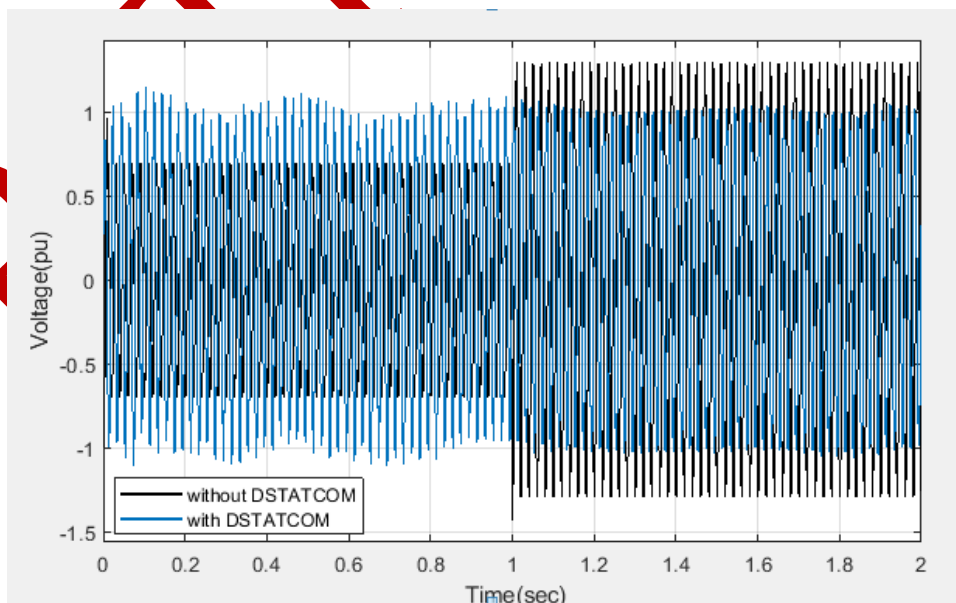

Figure 10. Voltage profile improvement for extreme sag event.

52

The technique that has been proposed is the use of ANN with PSO to regulate DSTATCOM for voltage profile improvement on distribution systems with the purpose of real-time control rather than traditional off-line control is an effective methodology. The controller was also tested for optimizing the voltage profile for continuous extreme sag and extreme swell, and the findings showed that the created controller was both resilient and efficient, as shown in Figs. 11 and 12 for rms and phase voltage, respectively.

Figure 11. Effect of developed DSTATCOM controller using AI on rms voltage profile

Figure 12. Effect of developed DSTATCOM controller using AI on instantaneous voltage profile

9. CONCLUSION

The results demonstrated the value of AI in DSTATCOM controller design, as the voltage profile is improved in real time during voltage events such as sag and swell. The PSO is used to find the best DSTATCOM controller gains, and then the ANN is utilized as an AI methodology to control DSTATCOM in real time. The effectiveness of employing ANN as an AI methodology to tune the PI controller of DSTATCOM in order to optimize the voltage profile on the distribution system was demonstrated in this study. The importance of AI approaches such as ANN was confirmed by the DSTATCOM with built controller. Using this designed controller, the power system's stability and dependability may be improved, and the network can become smart.

When compared to conventional control techniques, the developed controller using ANN enables DSTATCOM with a robust tuning system because it responds to various real-time voltage disturbances that may occur in the distribution system with efficient voltage profile augmentation. The simulation results showed that the suggested strategy for controlling DSTATCOM to improve the voltage profile on the distribution system is effective.

REFERENCES

[1] Z. Saafin, F. Zaro, M. Jawadeh, "Voltage Profile Improvement Using DSTATCOM Based on Artificial Intelligent Techniques," *IEEE Jordan International Joint Conference on Electrical Engineering and Information Technology (JEEIT)*, pp.773-778, 2019.

[2] A. Sharaf, F. Gandoman, "A switched hybrid filter-DVS/green plug for smart grid nonlinear loads," *Smart Energy Grid Engineering (SEGE)*, pp.1-6, 2015.

[3] T. Short, "Distribution reliability and power quality," United States: Crc Press, 2005.

[4] F. Zaro, M. Abido, "Real-Time Detection and Classification of Power Quality Problems Based on Wavelet Transform," *Jordan Journal of Electrical Engineering,* vol. 5, no. 4, pp. 222-242, 2019.

[5] O. Ipinnimo, S. Chowdhury, S.P. Chowdhury, J. Mitra, "A review of voltage dip mitigation techniques with distributed generation in electricity networks," *Electric Power Systems Research,* vol.103, pp. 28-36, 2013.

[6] A. Rana, I. Trivedi, C. Vasoya, M. Pandya, S. Gohil, P. Saradva, "Application of D-STATCOM for power quality improvement in distribution line," *International Conference on Computation of Power, Energy Information and Communication, Chennai*, pp. 719-725, 2016.

[7] S. Bhim, R. Sabha, V. Pankajkumar, "An implementation of double-frequency oscillation cancellation technique in control of DSTATCOM," *International Transactions on Electrical Energy Systems,* vol. 24, no. 6, pp. 796-807, 2013.

[8] C. Liu, Y. Hsu, "Design of a self-tuning PI controller for a STATCOM using particle swarm optimization," *IEEE Transactions on industrial Electronics,* vol. 57, no. 2, pp. 702-715, 2010.

[9] P. Kamaraj, T. Thamizharasu, "Voltage regulation of soft switched interleaved boost converter using fuzzy proportional integral controller," *Journal of Energy Systems*, vol. 4, no. 4, pp. 145-160, 2020.

[10] S. Alqam, F. Zaro, "Power Quality Detection and Classification Using S-Transform and Rule-Based Decision Tree," *International Journal of Electrical and Electronic Engineering & Telecommunications,* vol. 8, no. 1, pp. 45-50, 2019.

[11] M. Labeeb, B. Lathika, "Design and analysis of DSTATCOM using SRFT and ANN-fuzzy based control for power quality improvement," *IEEE Recent Advances in Intelligent Computational Systems, Trivandrum, Kerala,* pp. 274-279, 2011.

[12] A. Nabisha, X. Joseph, "Power Quality Enriched Wind Energy System using DSTATCOM based on PID-ANN Controller," *American-Eurasian Journal of Scientific Research,* vol. 12, no. 5, pp. 271-284, 2017.

[13] Babaei M, Jafari-Marandi M, Abdelwahed S, Smith B. A simulated Annealing-based optimal design of STATCOM under unbalanced conditions and faults. *Power and Energy Conference at Illinois (PECI),* pp. 1-5, 2017.

[14] F. Zaro, "True Multi-Objective Optimal Power Flow in a Deregulated Environment Using Intelligent Technique," *Journal of Engineering Research and Technology*, vol. 3, no. 4, pp. 110-118, 2017.

[15] S. Panda, N. Padhy, "Comparison of particle swarm optimization and genetic algorithm for FACTS-based controller design," *Applied soft computing*, vol. 8, no. 4, pp. 1418-1427, 2008.

[16] E. Beşikçi, O. Arslan, O. Turan, A. Ölçer, "An artificial neural network-based decision support system for energy efficient ship operations," *Computers & Operations Research,* vol. 66, pp. 393-401, 2016.

[17] S. Samadianfard, S. Jarhan, H. S. Nahand, "Application of support vector regression integrated with firefly optimization algorithm for predicting global solar radiation," *Journal of Energy Systems*, vol. 2, no. 4, pp. 180-189, 2018.